Pioneer GABA Cells Comprise a Subpopulation of Hub Neurons in the Developing Hippocampus

Michel A. Picardo, Philippe Guigue, Paolo Bonifazi, Renata Batista-Brito, Camille Allene, Alain Ribas, Gord Fishell, Agnès Baude, Rosa Cossart

Neuron
Article

Pioneer GABA Cells Comprise a Subpopulation of Hub Neurons in the Developing Hippocampus

Michel Aimé Picardo,[1,2,3] Philippe Guigue,[1,2,3] Paolo Bonifazi,[1,2,3,4] Renata Batista-Brito,[5] Camille Allene,[1,2,3] Alain Ribas,[1,2,3] Gord Fishell,[5] Agnès Baude,[1,2,3] and Rosa Cossart[1,2,3,*]
[1]Inserm Unité 901, Marseille 13009, France
[2]Université de la Méditerranée, UMR S901 Aix-Marseille 2, 13009, France
[3]INMED, Marseille 13009, France
[4]Beverly and Sackler Faculty of Exact Sciences School of Physics and Astronomy, Tel Aviv University, 69978 Ramat Aviv, Israel
[5]Smilow Neuroscience Program and the Departments of Cell Biology and Neural Science, NYU Langone Medical Center, 522 1st Avenue, New York, NY 10016, USA
*Correspondence: cossart@inmed.univ-mrs.fr
DOI 10.1016/j.neuron.2011.06.018

SUMMARY

Connectivity in the developing hippocampus displays a functional organization particularly effective in supporting network synchronization, as it includes superconnected hub neurons. We have previously shown that hub network function is supported by a subpopulation of GABA neurons. However, it is unclear whether hub cells are only transiently present or later develop into distinctive subclasses of interneurons. These questions are difficult to assess given the heterogeneity of the GABA neurons and the poor early expression of markers. To circumvent this conundrum, we used "genetic fate mapping" that allows for the selective labeling of GABA neurons based on their place and time of origin. We show that early-generated GABA cells form a subpopulation of hub neurons, characterized by an exceptionally widespread axonal arborization and the ability to single-handedly impact network dynamics when stimulated. Pioneer hub neurons remain into adulthood, when they acquire the classical markers of long-range projecting GABA neurons.

INTRODUCTION

One approach to unraveling the complexity of neuronal circuits is to understand how their connectivity emerges during brain maturation. Neuronal connectivity is very often reflected in the activity dynamics that a given network of neurons can produce. Interestingly, most developing neuronal networks spontaneously produce a variety of correlated activity dynamics that are thought to be essential for proper circuit maturation (Ben-Ari, 2001; Blankenship and Feller, 2010). At early postnatal stages, the hippocampus displays spontaneous, synapse-driven network synchronizations in the form of giant depolarizing potentials (GDPs) (Ben-Ari et al., 1989; Garaschuk et al., 1998). We have recently shown that, during this developmental period, the CA3 region displayed a "scale-free" functional topology (Bonifazi et al., 2009) characterized by the presence of rare, superconnected hub neurons. Hub neurons are characterized by the following features (Bonifazi et al., 2009): (1) they possess high output functional connectivity; (2) their stimulation significantly affects network dynamics (whereas stimulating other neurons does not); (3) they are GABA neurons with a widespread axonal arborization crossing subfield boundaries; and (4) they receive more excitatory postsynaptic potentials and have a lower threshold for action potential generation than other interneurons. Thus, the study (Bonifazi et al., 2009) confirmed the leading role of GABA neurons in shaping network oscillations (Ellender et al., 2010; Klausberger and Somogyi, 2008), that emerges as soon as the first functional synapses start to develop.

However, it is at present unknown whether hub neurons are only present transiently during development or if they persist into adulthood. If the latter, it is also unclear whether this population represents one or many morphophysiological subtypes of interneurons. Determining the subtypes of hub neurons is experimentally challenging for several reasons. First, hub neurons are a sparse cell population (Bonifazi et al., 2009). Second, cortical GABA neurons are characterized by a bewildering heterogeneity that results in several classification challenges. This complexity is further confounded during brain development by the fact that most GABA neurons have not yet developed the characteristics that enable investigators to identify and classify them in adulthood (Hennou et al., 2002). To address the above issues, it is essential to permanently label hub neurons in a manner such that they can be examined both for their dynamics during GDPs, as well as in the adult.

Based on the following arguments, we hypothesized that hub neurons could be early-generated interneurons (EGins) that pioneer hippocampal circuits. First, hub neurons were characterized by their advanced morphophysiological features compared to other developing GABA neurons (Bonifazi et al., 2009). Second, theoretical models predict that scale-free networks grow according to "preferential attachment rules," meaning that early connected neurons would turn into hub cells (Barabasi and Albert, 1999). In rodents, cortical GABA neurons are generated in the subpallium, mainly from two transient structures, the medial and caudal ganglionic eminences (Anderson et al., 1997;

Batista-Brito and Fishell, 2009; Marín and Rubenstein, 2001). Peak neurogenesis of hippocampal GABA interneurons in the mouse occurs between E12 and E15 (Danglot et al., 2006). However, some GABA neurons are postmitotic and start migrating as early as embryonic day 10 (Danglot et al., 2006; Miyoshi et al., 2007). From the above, we inferred that hub neurons may be generated during the earliest phases of neurogenesis. Interestingly, recent advances in molecular genetics have produced novel tools to control the permanent expression of green fluorescent protein (GFP) in the interneurons of transgenic mice in accordance with their spatio-temporal embryonic origin (Miyoshi and Fishell, 2006).

To test this hypothesis, we have performed a compound analysis of EGins, using a combination of genetic fate mapping (Miyoshi and Fishell, 2006) and immunohistochemistry coupled with imaging of network dynamics and single-cell electrophysiological recordings. We find that at early postnatal stages, EGins turn into a distinct functional subclass of hub neurons (Bonifazi et al., 2009). Furthermore, we show that EGins persist in adult hippocampal networks and express markers identifying them as putative long-range projecting GABA neurons (Jinno, 2009). This indicates that these cells may retain, at least anatomically, the capacity to coordinate the timing of neuronal activity across structures. Moreover, this finding provides the means to study the involvement of hub cells in other synchronization processes such as epilepsy (Morgan and Soltesz, 2008), independently from calcium data analysis.

RESULTS

EGins Develop into a Subclass of Interneurons with Widespread Axonal Arbors

Despite their varied sites of origin, most, if not all, hippocampal GABA interneurons require the expression of *Dlx1* and/or *Dlx2* for their generation, as evidenced by the near absence of GABA interneurons in *Dlx1/Dlx2* null compound mutants (Anderson et al., 1997; Bulfone et al., 1998; Long et al., 2009). Thus, in order to label as many EGins as possible we have fate mapped hippocampal interneuron precursors expressing *Dlx1/2*, by transiently activating a *Dlx1/2*^{CreERTM} driver line (Batista-Brito et al., 2008) crossed with a Cre-dependent EGFP reporter line *RCE:LoxP* (Sousa et al., 2009). Recombination of the reporter allele is achieved within 24 hr upon administration of tamoxifen, therefore providing temporal precision in the labeling of cells expressing *Dlx1/2* (see Experimental Procedures). Temporal control also requires *Dlx1/2* expression to be confined to postmitotic cells, as any labeling of progenitors would overtime produce labeled cells at later ages. This condition is satisfied by using the driver *Dlx1/2*^{CreERTM} because in this transgenic line *Dlx1/2* is only expressed shortly after interneurons become postmitotic (Batista-Brito et al., 2008). In order to further confirm the temporal resolution of our fate mapping approach at such unusually early force-feeding time period, we (1) performed a short term fate mapping of Dlx1/2 progenitors at E12.5 (induction at E7.5 or E9.5) and observed that GFP-positive cells could be detected along the lateral border of the ganglionic eminences, but excluded from the progenitor cell region lying in the embryonic ventricular zone (see Figure S1 available online). GFP-positive cells presented relatively developed processes (Figure S1C) and could even be found heading toward the hippocampal neuroepithelium, indicating an already advanced stage of migration (Figure S1C). We also (2) performed BrdU injections within a time window of 20 hr following tamoxifen force-feeding (at E9.5) and found significant GFP/BrdU colabeling in E12.5 embryos (28%, n = 1067 cells; Figures S1A and S1B) whereas a BrdU injection performed later than E10.5 did not result in any labeling of GFP cells (data not shown). This indicates that the EGins labeled here are likely to be born before E10.5.

We next analyzed the population of EGins using immunohistochemical approaches at two separate time points: early postnatal (P7) and adult stages (>P30). We first examined the distribution of GFP labeled cells within the adult hippocampus. Although a precise quantification of the density of EGins is impossible due to the variability in our labeling method, it is striking how few cells are labeled at these stages. Indeed, on average 4.8 ± 1.6 GFP neurons are present per hippocampal section in adult mice (n = 263 sections, seven mice; Figures 1A and 1B). On average, a similar number of GFP cells could be found at P7 (4.4 ± 1.2; n = 147 sections, seven mice; Figure 1C and Figure 2A), indicating that this subpopulation of cells is unlikely to experience massive developmental cell loss. The GFP reporter line used here provides the considerable benefit that after enhancement by immunohistochemistry, it produces a strong enough signal for the fine neuronal processes including axons to be examined. Although EGins represented only a few cells per hippocampal section, GFP axonal labeling displayed a remarkable web-like coverage of the entire hippocampal region in both age groups (Figures 1A and 1B and Figure 2A). Low-density but extensive axonal arbors were distributed in all hippocampal layers. However, no prominent axonal labeling could be found in the pyramidal cell layers (Figure 1B and Figure 2A), indicating that EGins were not principally targeting perisomatic regions. Axonal labeling was also frequently observed in the fimbria (Figure 2C). This is in marked contrast with the spatially patterned and confined labeling obtained when interneurons are fate mapped at later developmental time points (Figure 2B) or with a preferred perisomatic innervation like PV-expressing cells (Miyoshi et al., 2007). EGins could be multipolar or bipolar with horizontally or vertically oriented dendrites that, to a varying extent, were sparsely spiny (Figure 1, Figure 2, and Figure 3). Their somata were evenly found in all hippocampal areas (Figure 1 and Figure 2), with a slightly higher proportion of them being located in the hilar region of the dentate gyrus (Figures 1A and 1C). We also examined within each region, the laminar distribution of EGins. These were found in all layers but with a preference for the CA1 stratum oriens, CA3 stratum radiatum and hilar region of the dentate gyrus (Figure 1C). Similar layer distributions were found in P7 and P30 hippocampal sections (Figure 1C; $p < 0.05$ Kolmogorov-Smirnov test).

Interestingly, both the regional distribution and axonal pattern of EGins were reminiscent of those reported for interneurons with an extrahippocampal projection (Jinno et al., 2007) (Figure 1). This subclass of interneurons was studied in great detail using immunohistochemical approaches (Gulyás et al., 2003; Jinno, 2009; Takács et al., 2008) and was proposed to serve a

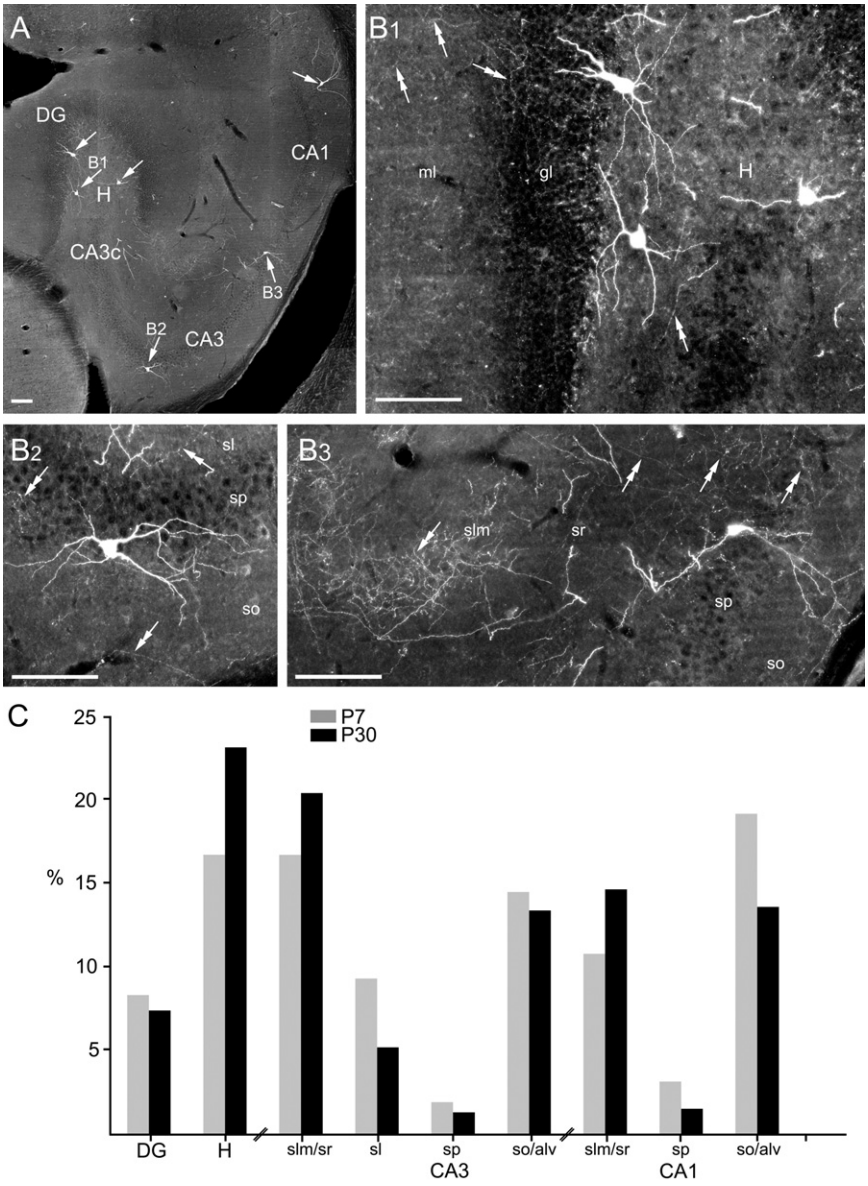

Figure 1. The Distribution of EGins in Horizontal Sections of the Hippocampus in P7 and Adult Mice

(A and B) Fate-mapped sparse neurons (arrows) are visible all over the hippocampus after GFP immunoperoxidase detection in a P30 tamoxifen-treated at E7.5 *Dlx1/2*^{CreERTM}*;RCE:LoxP* mouse. B1-3 are enlargements of the areas indicated in A showing the multipolar feature of labeled somata and their relative extensive dendritic arborization. Axonal processes (double arrows) can be observed in all layers of the dentate gyrus (DG) and hilus (B1), CA3 (B2) and CA1 (B3) areas.

(C) Histogram reporting the fraction of EGins present in different hippocampal layers of P7 (410 cells, n = 7 pups) and P30 (963 cells, n = 5 mice) tamoxifen-treated *Dlx1/2*^{CreERTM}*;RCE:LoxP* animals. Alv, alveus; gl, granular layer; H, hilus; ml, molecular layer, slm, stratum laculosum moleculare; sr, stratum radiatum; sl, stratum lucidum; sp, stratum pyramidale; so, stratum oriens. Scale bar represents 100 μm.

hub function through an axon targeting distant regions (Buzsáki et al., 2004; Sik et al., 1994, 1995).

We next immunostained hippocampal sections containing EGins with a variety of classic interneuron markers. Given the late maturation of interneurons' neurochemical content, only sections from adult mice were included here. Although parvalbumin (PV), calbindin (CB), vasoactive intestinal peptide (VIP), calretinin (CR), or nitric oxide synthase (NOS) are prominently expressed by most hippocampal interneuron classes, almost none of the EGins were positive for these markers (Figures 3B and 3G–K). In contrast, a significant fraction of them were immunopositive for somatostatin (SOM) (45% ± 6%, n = 9 animals; Figures 3A and 3L). SOM-expressing hippocampal interneurons constitute a heterogenous population that includes O-LM and HIPP cells, hippocampo-subicular and hippocampo-septal projection neurons (Jinno et al., 2007) as well as bistratified interneurons. In addition to SOM, O-LM cells also express PV (Ferraguti et al., 2004) and receive strong VIP positive inputs (Acsády et al., 1996). None of the EGins was positive for both SOM and PV (Figures 3C–3E and Figure S2B). Moreover, EGins did not receive strong VIP positive inputs (Figure S2A). Therefore, we can exclude that a large number of EGins become O-LM cells. Given this last result and the fact that the distribution and axonal arborization pattern of EGins resembled that of long-range projecting neurons, we next tested for the expression of mGluR1α and M2 receptor, both being additional characteristic markers of interneurons with extrahippocampal projections (Jinno et al., 2007). We found that a large majority of EGins was positive for mGluR1α (72.2% ± 7.7%, n = 5 mice; Figures 3A and 3L) and that a significant fraction of them expressed the M2 receptor (18.4% ± 2.5%, n = 4 mice; Figures 3F and 3L). In addition we tested for the coexpression of SOM and mGluR1α and found that 53.4% ± 7.5% (n = 4 mice) of EGins coexpressed both markers, further indicating a long-range projecting phenotype. Because neurochemical marker expression is developmentally regulated, systematic testing and quantification of their presence within EGins was difficult to assess at P7. Nevertheless, SOM, mGluR1α, and M2 receptor immunoreactivities were found in EGins at early postnatal stages (Figures 2D–2F). In order to further exclude that EGins develop into basket-like or O-LM interneurons, we have patch-clamped and filled with neurobiotin EGins focusing on the CA3 region of slices prepared from adult mice (P25, n = 65 neurons). Out of 65 filled cells 38 were sufficiently recovered and 12 reconstructed. None of these cells showed any axonal or

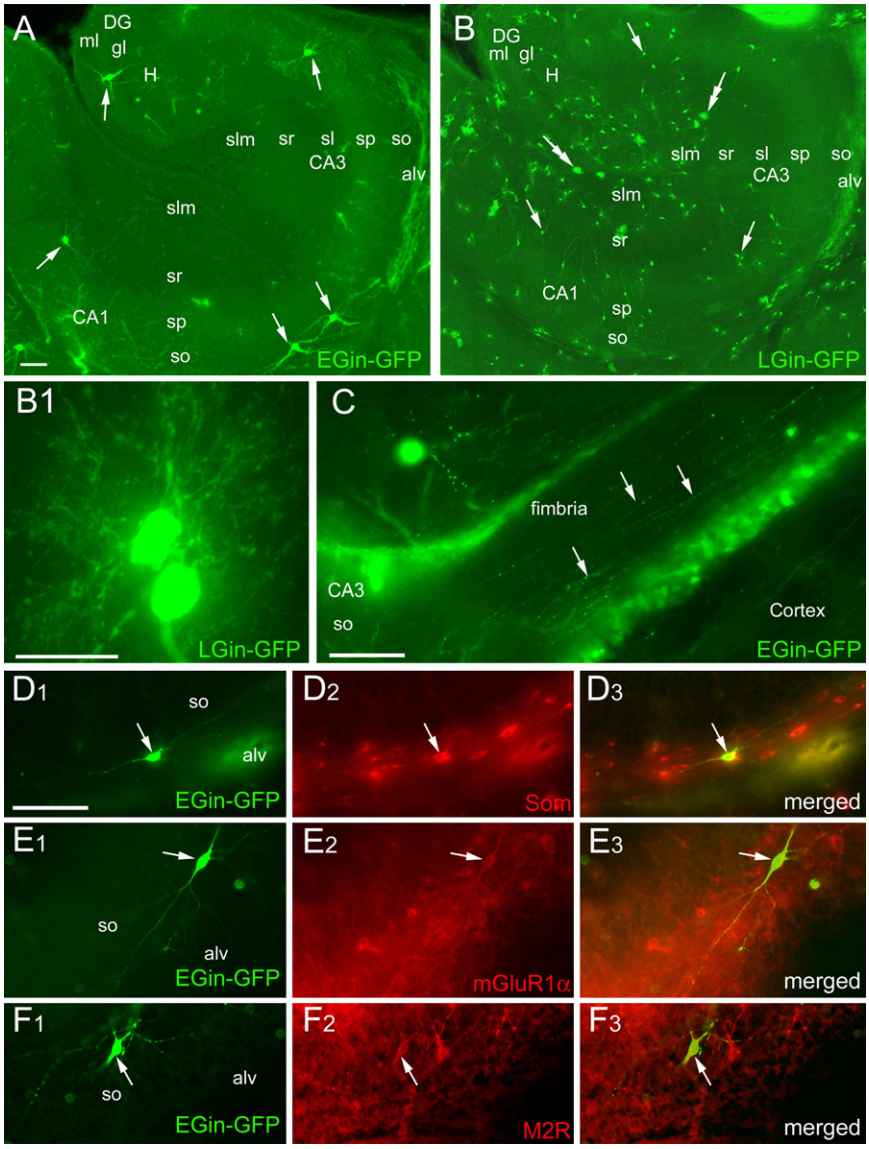

Figure 2. The Morphological and Neurochemical Properties of EGins in Horizontal Sections of the Hippocampus at P7

(A and B) Distribution of GFP-expressing early-generated neurons (EGins, induction: E7.5) and late generated neurons (LGins) in horizontal sections of the hippocampus of P7 mice. EGins (arrows in A) represent a sparse population compared to the numerous LGins (arrows and double arrows in B). LGins are present in all hippocampal layers but are predominantly located in stratum pyramidale (sp) and stratum lacunosum-moleculare (slm). Several LGins exhibit morphological features resembling neurogliaform cells (double arrows in B and B1). Scale bar in (B1) represents 20 μm.

(C) GFP-positive axons are running along the fimbria (arrows) in EGins-GFP mice.

(D–F) Examples of immunofluorescence for SOM, mGluR1α, and M2R in EGins within CA3 stratum oriens (so). alv, alveus; DG, dentate gyrus; gl, granular layer; H, hilus; ml, molecular layer; sl, stratum lucidum; sr, stratum radiatum. Scale bar represents 100 μm.

dendritic characteristics of O-LM or perisomatic interneurons (Figure S3). In contrast, despite some heterogeneity, they shared a remarkable common property with previously filled GABA projection neurons in the CA1 region of hippocampal slices as their axon tended to run out of the slice before giving off any terminal arbor (Gulyás et al., 2003). In addition, their evoked firing pattern could be classified either as irregular/stuttering (34%, n = 26, data not shown) or burst adapting (46%, n = 26; Figure S3). None of them were fast spiking. The latter further excludes that EGins develop into basket-like interneurons.

To conclude, morphological analysis of EGins indicated that these cells provide wide axonal coverage to the hippocampus at early postnatal stages (P7) and that a majority of them acquire morphological characteristics of GABA projection neurons in adulthood. Because long-range and widespread axonal arborization constitute a characteristic feature of previously described hub neurons (Bonifazi et al., 2009), we next tested whether these cells developed into functional hubs at early postnatal stages (P5–P7).

EGins Display Morphophysiological Characteristics Comparable to Previously Described Hub Neurons

We first compared the morphophysiological features of EGins to those previously observed in functional hub neurons (Bonifazi et al., 2009). As in our previous study (Bonifazi et al., 2009), we decided to focus on the CA3c hippocampal region as it is a preferred initiation site for GDPs (Menendez de la Prida et al., 1998). Previously described functional hubs could be distinguished by four times longer axonal lengths than low connectivity interneurons, a lower threshold for action potential generation, and more frequent spontaneous excitatory postsynaptic potentials (sEPSPs) (Bonifazi et al., 2009). While being recorded at P5–P7, genetically-labeled GFP-positive cells from tamoxifen-treated *Dlx1/2*^{CreERTM}*;RCE:LoxP* mice were filled with neurobiotin (n = 56 cells). Different types of morphologies could be recovered (Figure 4A). Twenty cells were reconstructed for morphometric analysis (Figure 4 and Figure 5). Out of all the parameters included in the analysis (see Experimental Procedures, Figure 4, and Figure 5), EGins were most identifiable by their axonal length (average: 8241 ± 1947 μm, n = 20 cells). A measure of their extended axonal coverage is the distribution of the number of intersections their axon makes with concentric circles of increasing radius centered at the soma (Sholl analysis; see Experimental Procedures and Figure 5B). The pooled distribution of the number of intersections as a function of distance from the soma, for all reconstructed EGins, is long-tailed

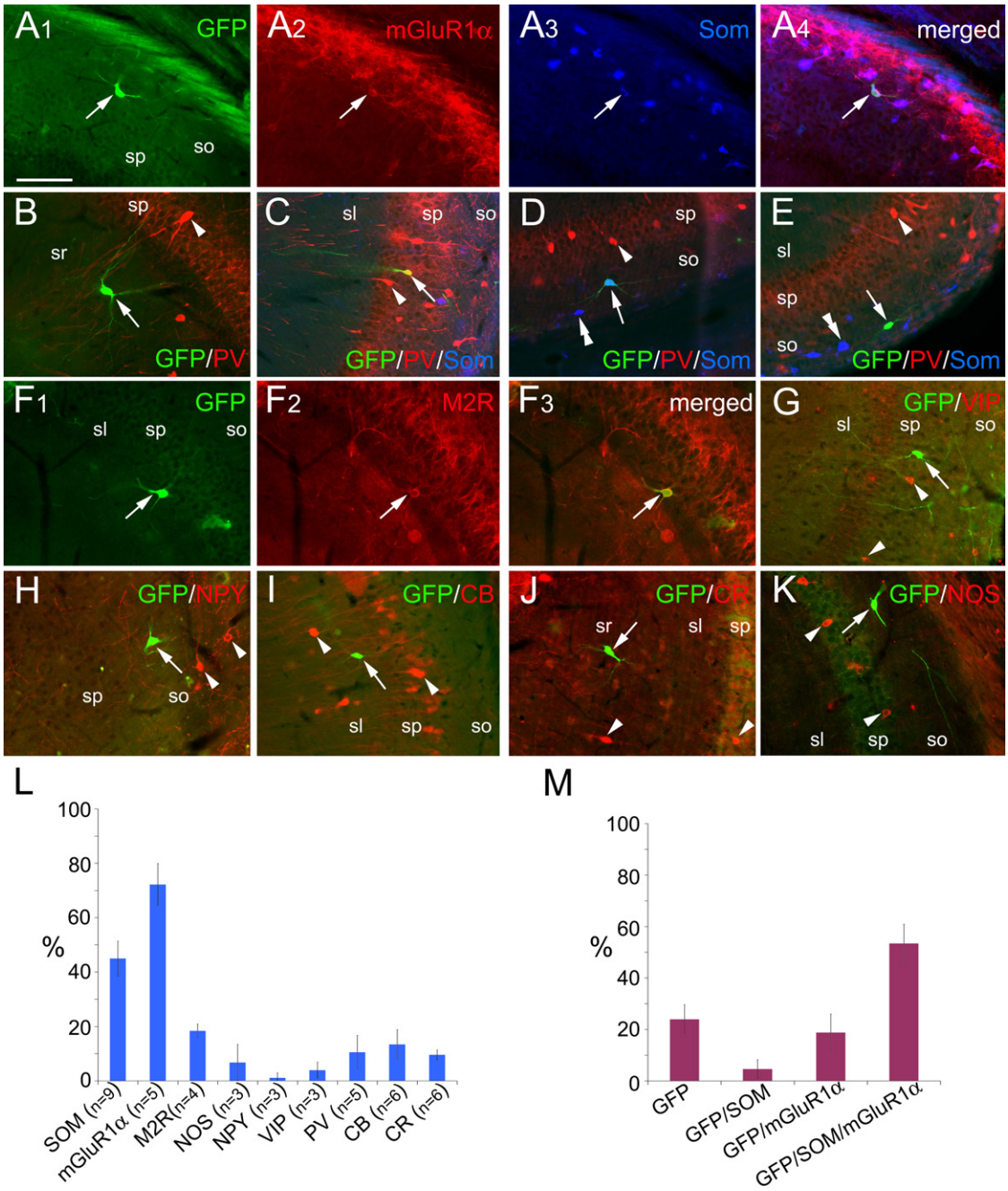

Figure 3. SOM and mGluR1α Are Preferentially Expressed in EGins in the Adult Hippocampus

All images are from the CA3 area. All GFP-positive neurons correspond to EGins labeled using tamoxifen-treated *Dlx1/2*^{CreERTM}*;RCE:LoxP* mice (induction: E7.5).

(A) A GFP-positive EGin (arrow) coexpressing mGluR1α and SOM in the CA3 stratum oriens.

(B–E) Generally, EGins do not express PV (arrows in B, D, E) even though very occasional PV positive cells can be seen (arrow in C). GFP-positive cells never coexpress PV and SOM (arrows in C–E) but can be observed next to cells that are positive for PV or SOM (single or double arrowheads). Note that the GFP cell in D (arrow) is colabeled for SOM.

(F) M2R labeling in a GFP-positive cell (arrows).

(G–K) In the vast majority of fate-mapped GFP-positive cells (arrows), neither immunoreactivity (arrowheads) for VIP, nor for NPY, CB, CR, or NOS is detected.

(L) Histogram showing the fraction of EGins immunoreactive for the various tested molecular markers. Note that two-thirds and almost half of the EGins contain mGLuR1α and SOM, respectively. [n], number of tested mice.

(M) In triple labeled sections, most of the GFP and SOM positive cells are also labeled for mGluR1α. Few EGins are mGluR1α positive only, and even fewer only SOM positive. A few EGins were immunonegative for both markers. Data were obtained from four tamoxifen-treated *Dlx1/2*^{CreERTM}*;RCE:LoxP* mice. sl, stratum lucidum; sp, stratum pyramidale; so, stratum oriens. Scale bar represents 100 μm.

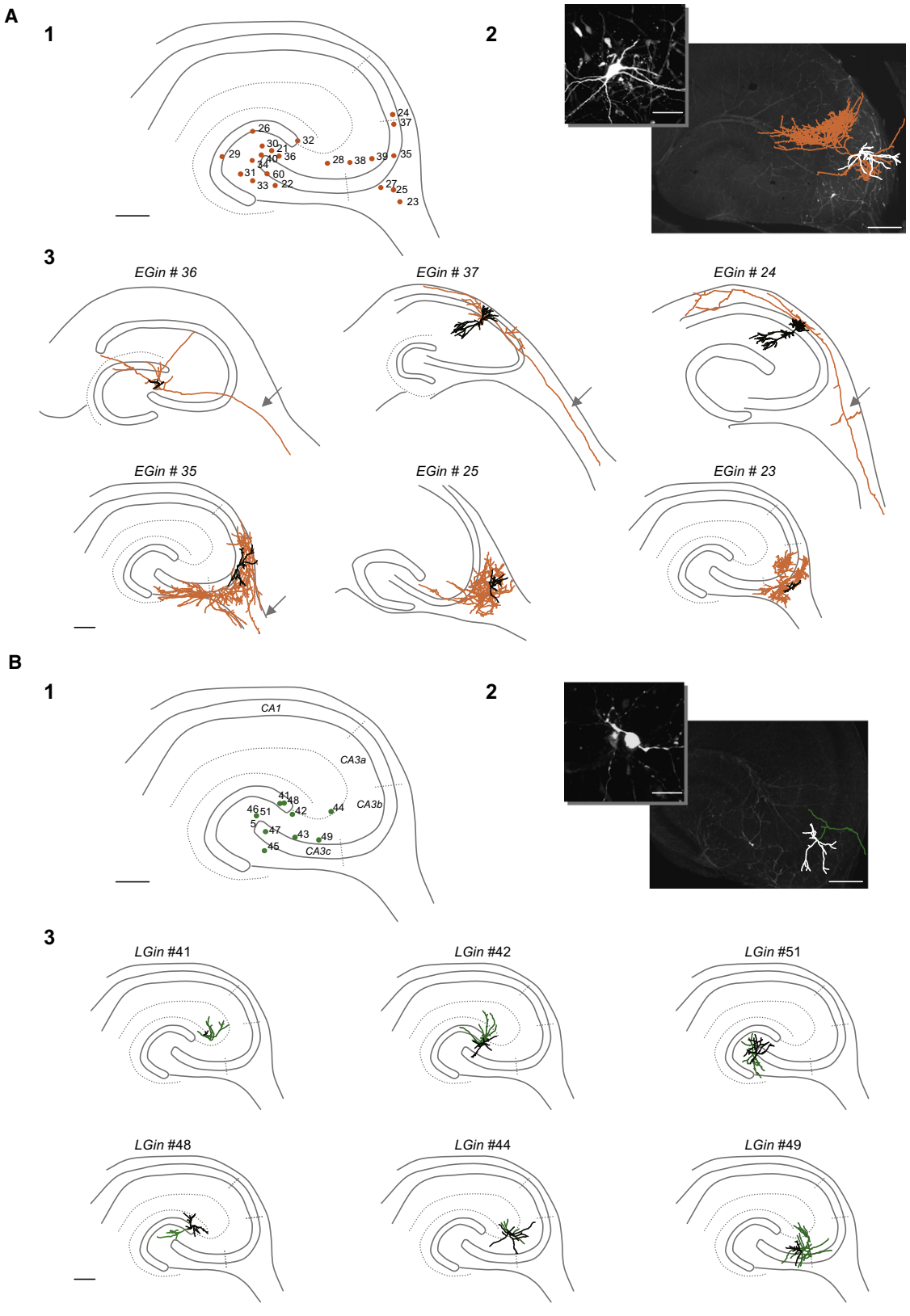
A
1
2
3
EGin # 36
EGin # 37
EGin # 24
EGin # 35
EGin # 25
EGin # 23
B
1
2
3
CA1
CA3a
CA3b
CA3c
LGin #41
LGin #42
LGin #51
LGin #48
LGin #44
LGin #49

because it is best fitted by a log-normal function (median: 250 ± 4 μm, R^2 = 0.99; Figure 5B), whereas the same plot for interneurons with a different embryonic origin is best fitted by a sum of two Gaussian distributions (see below and Figure 5B). Pooling data from previously sampled hub neurons (Bonifazi et al., 2009) presented a similar log-normal distribution of axonal intersections (median: 227 ± 5 μm, R^2 = 0.98, Figure 5B). In fact, none of the morphometric measurements obtained for EGins was significantly different from previously sampled functional hub neurons. Indeed, we performed a multivariate cluster analysis (see Experimental Procedures) of the morphometric data of 20 EGins, 10 hubs (high connectivity [HC]) (cf. Bonifazi et al., 2009), 10 low connectivity (LC) neurons (cf. Bonifazi et al., 2009), and 11 GABA neurons with a protracted origin (late generated interneurons [LGins]; see below) and found that EGins and hub neurons significantly clustered into the same group (Figure 5C). Moreover, like functional hubs, the axonal coverage of EGins often crossed subfield boundaries. Axonal branches from 20% neurons could be seen running in the fimbria (Figure 4A), possibly indicating an extrahippocampal projection at early postnatal stages. Within the hippocampus, axons arborized uniformly in all hippocampal layers with the exception of stratum pyramidale, which showed little axonal innervation (Figure 4A). This is in agreement with the immunolabeling results that rules out the possibility that this population is predominantly comprised by PV-containing perisomatic cells. Regarding the basic electrophysiological features analyzed here (see Figure 6), we found that EGins received a high frequency of sEPSPs and had a low threshold for action potential generation. These properties were significantly different from those recorded in LGins ($p < 0.05$) but not from those measured in functional hub cells (Figure 6; Student's t test, $p > 0.1$). Taken together, these results indicate that EGins display morpholo-physiological characteristics that are exceptional similar to previously described functional hub neurons.

LGins Do Not Display Hub-Like Morphophysiological Features

Because this study focuses on the embryonic origin of neurons, we decided to compare EGins with LGins labeled with a similar inducible genetic approach. Due to their relatively late birth dates (Miyoshi and Fishell, 2011), we decided to focus on CGE-derived interneurons by combining the Mash1BAC-CreER driver with the RCE:loxP reporter. By chance, this line broadly labels Mash1-expressing cells in CGE and lateral ganglionic eminence, but not within the MGE (Miyoshi and Fishell, 2011). In order to restrict GFP labeling to LGins, we force-fed tamoxifen to pregnant transgenic mice at late embryonic stages. GFP labeling in hippocampal sections from P7 Mash1 mice given tamoxifen at E18, indicated that LGins displayed variable morphologies, including a neurogliaform dendritic anatomy (Figure 2B), in agreement with the previously described CGE origin of NOS-negative neurogliaform cells (Tricoire et al., 2010). Their different morphology aside, the hippocampal distribution and density of LG- and EGins were quite distinct, as LGins were numerous with a high density in the CA1 and CA3c stratum lacunosum-moleculare and absence from CA3b (Figures 2A and 2B). In order to further describe their morphometric features, LGins were filled with neurobiotin and processed post hoc. Variable morphologies could be recovered and reconstructed (n = 11; Figure 4B). Axonal length was highly variable (range: 77–3826 μm; Figure 5A) but on average significantly shorter than that of previously recorded low connectivity interneurons (Bonifazi et al., 2009). Moreover, both interneuron samples clustered into the same group, which was distinct from hub and EGins (Figure 5C). Regarding basic electrophysiological properties, LGins were comparable to low connectivity interneurons (see Figure 6). We conclude that in contrast to EGins, LGins originating from the CGE present much less developed morphophysiological features. We next compared the network functional connectivity of EGins and LGins in order to determine whether EGins could become functional hubs at early postnatal stages.

EGins Become Functional Hub Neurons for the Generation of GDPs in the CA3 Hippocampal Region

To test whether EGins become functional hubs, we performed multineuron calcium imaging of hippocampal slices from tamoxifen-treated *Dlx1/2*^{CreERTM}*;RCE:LoxP* mice, focusing on CA3c, the region where functional hubs tended to concentrate. Interestingly, GFP labeling was rather frequent in that area (cf. above and Figure 1). Unfortunately, for unknown reasons, GFP-positive cells could not be efficiently labeled with the calcium-permeable indicator used here (Fura2-AM) that precluded calculating their functional connectivity index based on the analysis of their spontaneous calcium events. Nevertheless, a distinctive feature of functional hub neurons (even more striking than their high functional connectivity index) was their higher "effective connectivity" as compared to any other neuron, including high

Figure 4. Morphological Features of Early- and Late-Generated Hippocampal GABA Interneurons

(A1) Distribution of the somatic location of all morphologically recovered EGins (n = 21) on a schematic representation of the hippocampus. All these cells correspond to GFP-positive neurons in tamoxifen-treated *Dlx1/2*^{CreERTM}*;RCE:LoxP* mice that were filled with neurobiotin and processed post hoc. Scale bar represents 200 μm.

(A2) Photomicrograph at low (scale bar represents 200 μm) and high magnification (inset: scale bar represents 50 μm) of the confocal image of a neurobiotin filled EGin. Neuronal morphology was analyzed between P5 and 7. Tamoxifen was provided at E7.5 except for cell 23 for which induction occurred at E9.5. The Neurolucida reconstruction of the cell is superimposed and shows a dense and widespread axonal arborization (orange). Soma and dendritic arborization are white.

(A3) Neurolucida reconstructions of six representative EGins. Note that despite their variable morphological features, all these cells display a long axonal arborization (orange) spanning across hippocampal layers. Axons may present a dense arborization (e.g., cells 35, 25, and 23) and/or a long branch often running toward the fimbria (arrow in cells 36, 37, 24, and 35). Scale bar represents 200 μm.

(B) Same as (A) but for LGins (n = 9) corresponding to neurobiotin-filled GFP-positive neurons from P5-7 *Mash1*^{CreERTM}*;RCE:LoxP* mice tamoxifen-treated at E18.5 (see Experimental Procedures). Note that the axonal arborization (green) of these cells is more confined and less ramified than that of early-generated neurons. Scale bar represents 200 μm.

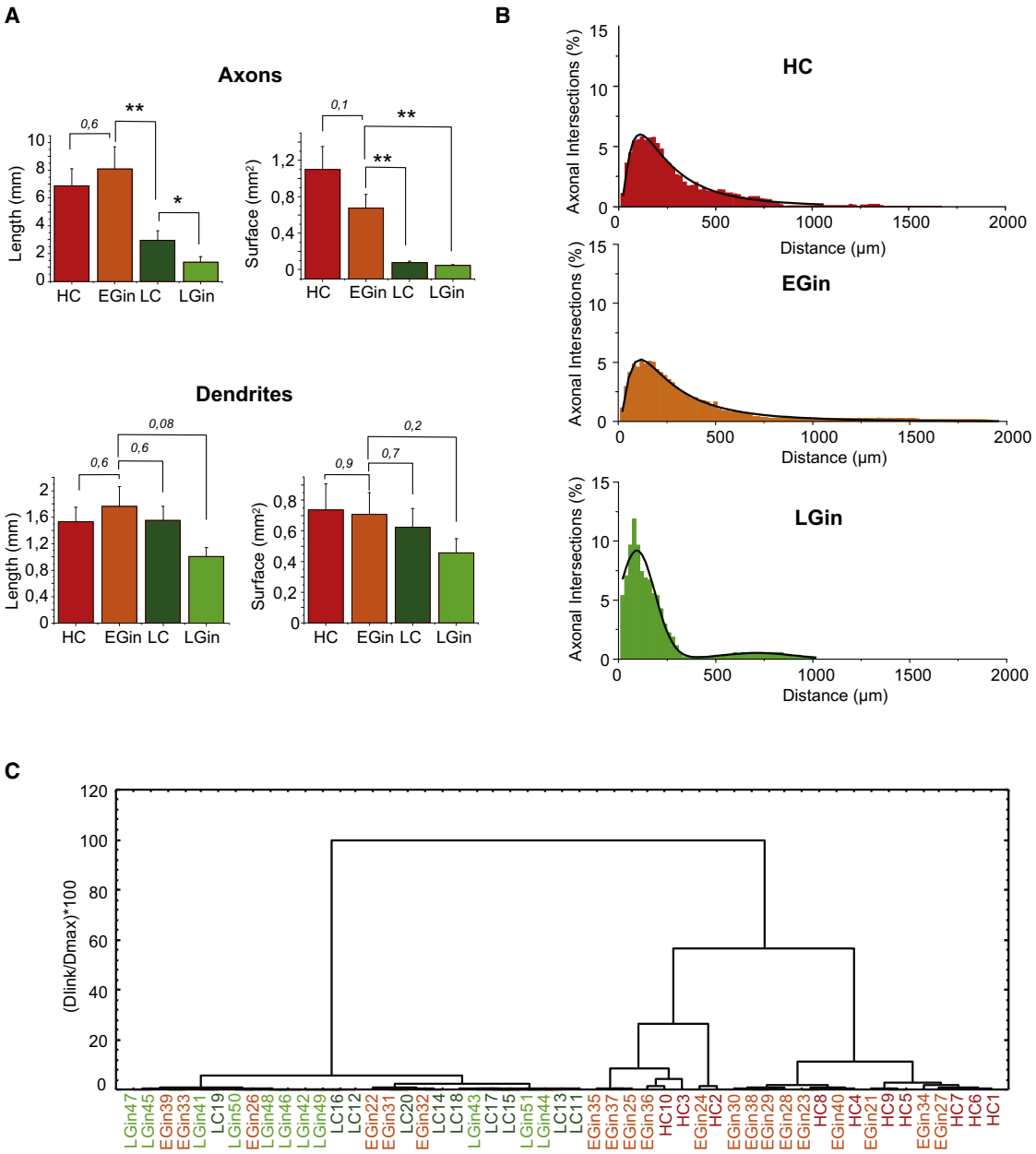

Figure 5. EGins Display Remarkable Morphometric Features Similar to Those of Hub Neurons

(A) Bar graphs comparing the averaged axonal (top) and dendritic (bottom) lengths (left) and surfaces (right) obtained in Neurolucida reconstructed high-connectivity (HC, red, n = 10; Bonifazi et al., 2009), early-generated (EGin, orange, n = 20), low-connectivity (LC, dark green, n = 10; Bonifazi et al., 2009) and late-generated (LGin, light green, n = 10) interneurons. *p < 0.05, **p < 0.001.

(B) Normalized distribution graphs of the fraction of axonal intersections with concentric circles of increasing radius (20 µm steps) centered at the soma for the cell populations described in (A) (same color code). Distributions obtained for HC and EGins are best fitted by a log normal function (black) indicating heavy tailed distributions whereas LGins are best fitted by two Gaussian functions (black).

(C) Cluster analysis tree of the morphological variables describing the same cells as in (A) (Ward's method, Dlink: Euclidian distances; see Experimental Procedures). Distances were normalized. Most HC and EGins segregated in the same group whereas LC and LGins segregated in another.

functional connectivity pyramidal cells (Bonifazi et al., 2009). Effective connectivity maps can be determined by calculating the average calcium fluorescence change across trials in every imaged cell following the stimulation of a single one. To build the effective connectivity maps of EGins and LGins, we targeted and recorded in current-clamp conditions, GFP-positive neurons (n = 56 cells) and stimulated them by intracellular current injections while imaging single-cell calcium responses in other imaged neurons (see Experimental Procedures). We observed that EGins displayed effective connections with 43% ± 10% of

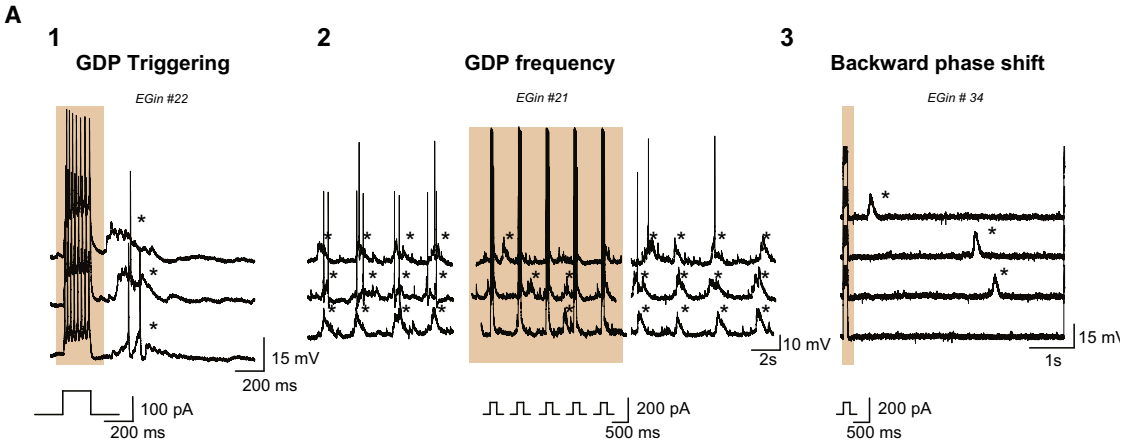

B

Properties	*EGin*	*LGin*	*HC*
Vrest (mV)	-47± 2	-39 ± 1 p<0.01	-54 ± 3 p=0.1
Rinput (Mohms)	663 ± 68	651 ± 75 p=0.7	380 ± 6 p=0.05
Capacitance (pF)	61 ± 10	61 ± 7 p=0.0.4	65 ± 17 p=0.9
Vthresh (mV)	-43 ± 1	-38 ± 1 p<0.001	-44 ± 3 p=0.6
AP width (ms)	2.3 ± 0.2	2.2 ± 0.1 p=0.6	2.1 ± 0.5 p=0.2
AP amplitude (mV)	49 ± 3	36 ± 2 p<0.001	45 ± 6 p=0.5
sEPSP frequency (Hz)	3.6 ± 0.5	2.3 ± 0.2 p<0.05	4.5 ± 1.5 p=0.7
sEPSP amplitude (mV)	3.5 ± 0.3	2.1 ± 0.1 p<0.001	2.2 ± 0.4 p=0.01

Figure 6. Electrophysiological Characteristics of EGins

(A) Current clamp traces of EGins recorded at resting membrane potential during stimulation (orange) corresponding to the same cells as illustrated on Figure 8B.
(A1) Three trials showing a stimulation (square pulse below) followed by a polysynaptic membrane potential depolarization characteristic of GDPs (denoted by *).
(A2) The frequency of GDPs (denoted by *) is significantly reduced during stimulation (indicated by square pulses below).
(A3) Current-clamp recordings from four consecutive stimulation trials (square pulse) show the progressive delay in the occurrence of a GDP (*) following stimulation (orange).
(B) Table comparing basic electrophysiological measurements obtained in EGins, LGins, and previously sampled high connectivity (HC) hub cells. P values obtained when comparing EGins with LGins or HC cells are indicated (Student or Mann-Whitney tests). V_{rest}, resting membrane potential; R_{input}, input resistance; $V_{threshold}$, action potential threshold; AP width, action potential width measured at half maximal amplitude; AP amplitude, action potential amplitude; sEPSP, spontaneous excitatory postsynaptic potentials.

active cells (n = 8 cells; Figure 7), whereas LGins displayed a significantly lower effective connectivity index (10% ± 5%, n = 6 cells, $p < 0.05$, Mann-Whitney; Figure 7).

To further test the contribution to network dynamics of EGins, we tested their influence on spontaneous network dynamics in the form of GDPs. Of those examined, only 32 experiments are considered here (see Experimental Procedures).

A phasic stimulation protocol was applied, i.e., short suprathreshold current pulses repeated at 0.1 to 0.2 Hz (the frequency range of GDP occurrence). As previously described (Bonifazi et al., 2009), cell/network interaction was estimated using three metrics: (1) the frequency of occurrence of spontaneous network synchronizations (GDPs) during the stimulation relative to the resting condition; (2) the peristimulus time histogram plotting the average fraction of cells activated by the phasic stimulation; and (3) forward/backward GDP phase shifts relative to a harmonic oscillator mimicking GDPs rhythm in resting conditions; in this way the number of observed versus expected GDPs was estimated over time. A cell was considered as affecting network dynamics significantly if it satisfied any of the above criteria. Remarkably, when stimulated, a very large majority of EGins (72%, n = 23 cells, Figure 6A and Figures 8A and 8B) significantly affected network dynamics as follows. (1) In 48% cases the average GDP frequency was altered during stimulation because inter-GDP interval distributions were statistically different in control conditions and during stimulation ($p < 0.05$, Student's t test or Mann-Whitney test, see Experimental Procedures). Twenty-six percent EGins decreased GDP frequency to

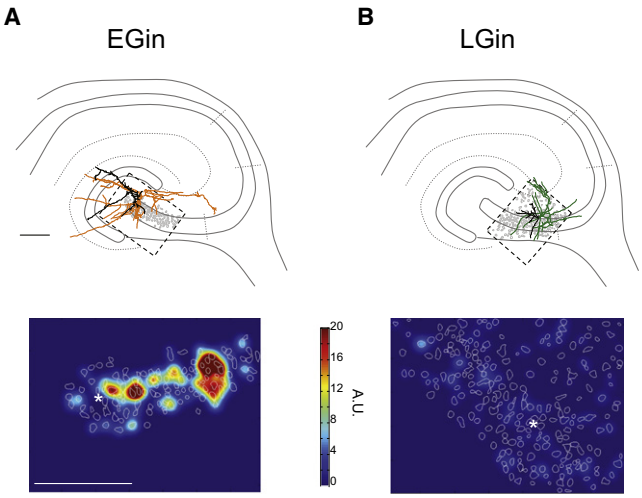

Figure 7. EGins Cells Display a High Effective Connectivity

(A) Neurolucida reconstruction of a CA3c EGin (induction: E9.5, analysis: P6) on a schematic representation of the hippocampus reveals an extended axonal arborization (orange, dendrites and soma in black) Black rectangle marks the imaged region and includes the contour map of imaged cells (gray). Image below is a color coded representation of the effective connectivity map (see Experimental Procedures). The asterisk indicates the cell body position. Red color represents high density of effective targets (A.U., arbitrary units). This EGin therefore displays a high effective connectivity.

(B) Same as (A), but for a representative LGin (induction: E18.5, analysis: P6). Note that stimulation of that cell does not induce any significant calcium response in other imaged neurons, even though the axonal arborization (green) of that LGin was fairly developed. Scale bar represents 200 μm.

78% ± 8% of control whereas 22% increased GDP frequency to 176% ± 26% of control. (2) In 48% of the cases, phasic stimulation triggered network synchrony in the form of GDPs in 32% ± 4% of the trials within 1 s after the stimulus (probability p that these events occurred by chance or due to the intrinsic periodicity of GDPs was <0.05; see Experimental Procedures). (3) Phasic stimulations induced a forward or backward GDP phase shift as compared to resting conditions, in 52% and 26% of the cases respectively ($p < 0.01$, see Experimental Procedures) EGins often displayed more than one form of cell/network interaction because 56% of them significantly affected network dynamics according to at least two of the above criteria ($p < 0.05$). Previous description of functional hub cells (Bonifazi et al., 2009) indicated that only stimulating GABA hub neurons could similarly affect network dynamics. In addition, whatever their axonal morphology (see precedent chapter), EGins have impact on the network activity (see Figure 8). Accordingly, in contrast to EGins, none of the LGins showed any significant effect according to the three metrics described just above (Figure 8C, $n = 7$, $p > 0.05$).

This evidence therefore shows that EGins act as functional hubs for the generation of GDPs.

DISCUSSION

The developing hippocampal network comprises a functional family of GABA hub interneurons essential for synchronization (Bonifazi et al., 2009). Here we find that a subpopulation of hub cells includes the GABA neurons that are generated earliest from the embryonic ganglionic eminences. This subpopulation of hub neurons is maintained throughout adulthood when a significant fraction of them expresses characteristic markers for GABA projection neurons (Gulyás et al., 2003; Jinno et al., 2007; Jinno, 2009). Thus our findings suggest at least anatomically, that hub cells are retained in adulthood, raising the possibility that hub function may be similarly preserved. Previous studies have identified pioneer neurons, including Cajal Retzius and subplate neurons, that contribute to the establishment of cortical networks (Del Río et al., 1997; Ghosh and Shatz, 1992; Kanold and Luhmann, 2010; Kanold and Shatz, 2006; Supèr et al., 1998). We identify a new population of GABA pioneer neurons with intriguing developmental functionality, and that, unlike most pioneer neurons (Kanold and Luhmann, 2010; Meyer et al., 1998; Price et al., 1997; Supèr et al., 1998) persist into adulthood.

EGins Are Hub Neurons that Function in the Generation of GDPs

The conclusion that GABA EGins are largely synonymous with previously defined hub neurons (Bonifazi et al., 2009) is supported by several lines of evidence. First, as theoretically defined (Boccaletti et al., 2006) and experimentally verified (Bonifazi et al., 2009), hub neurons should comprise a small proportion of cells: precisely as EGins do. Second, unbiased multiparametric analysis of morphometric data indicate that EGins are physically similar to hub neurons, the cardinal feature being a widespread axonal morphology. Third, the fundamental electrophysiological features of EGins are comparable to hub neurons. Fourth, EGins possess a high effective connectivity index because their stimulation leads to the activation of many neurons. Notably, high effective connectivity is more predictive of a hub cell identity than a high "functional connectivity." For example, pyramidal cells could display a high functional connectivity without being functional hub neurons as their effective connectivity was low and stimulating them did not affect network dynamics (Bonifazi et al., 2009). Given the intrinsically limited temporal resolution of calcium imaging approaches, the latter criterion is undoubtedly the most stringent experimental test for a hub neuron.

Morphophysiological Characteristics of Early-Generated GABA Hub Neurons

Early-generated GABA hub neurons resemble previously termed "connector" hubs rather than the basket-like subtype (Bonifazi et al., 2009; Bullmore and Sporns, 2009) and are therefore more likely to be classified as dendritic- rather than somatic-targeting interneurons as indicated by their preferential expression of SOM. This is consistent with the paucity of PV expression, the most common marker for somatic-projecting interneurons. Indeed, their axons preferentially arborized in the dendritic layers rather than in the pyramidal cell layer. The fact that EGins largely innervate dendritic layers is also in agreement with the earlier development of GABA synapses in these layers (Gozlan and Ben-Ari, 2003). In addition to SOM, the majority of EGins express mGluR1α and, to a lesser extent, M2R. By contrast, PV, VIP and

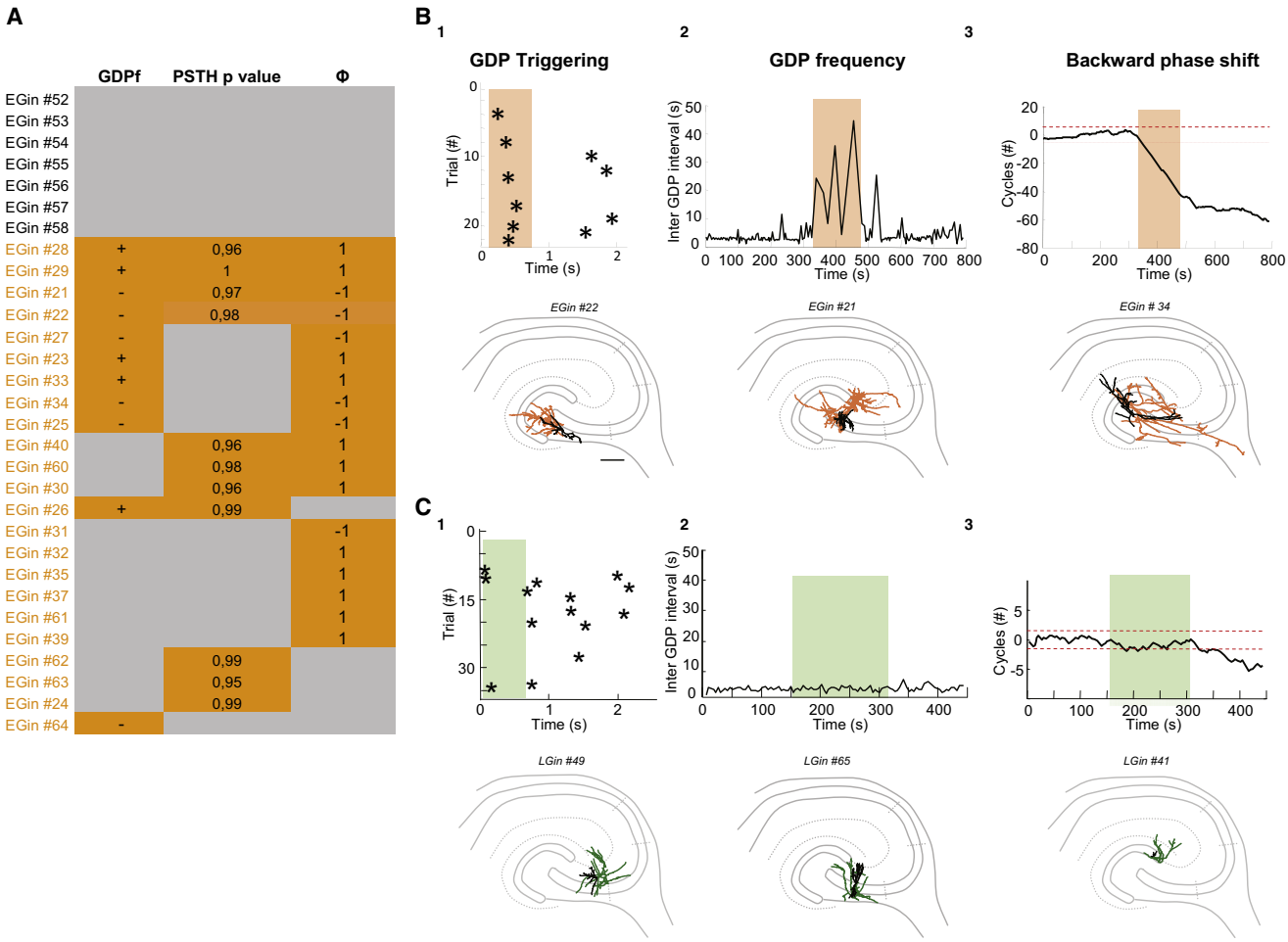

Figure 8. Stimulation of Early- But Not Late-Generated Interneurons Significantly Perturbs Network Dynamics

(A) Summary table of the effects on network dynamics after stimulating EGins. Significant results are displayed in orange whereas gray boxes indicate no effect. Columns indicate the three possible types of effects (illustrated in B): (1) increase (+) or decrease (−) of GDP frequency (GDPf); (2) GDP triggered after stimulation (p value obtained after statistical analysis of the peristimulus time histogram (PSTH) is indicated; and (3) forward (1) or backward (−1) phase (Φ) shift.

(B) Three types of effects on network dynamics observed in response to repetitive phasic stimulation of EGins. Tamoxifen induction: E9.5 (cells 22 and 21), E7.5 (cell 34). Analysis: P6–P7.

(B1) GDP triggering. GDP occurrence (indicated by *) as a function of time following repetitive phasic stimulation of a representative EGin (22 consecutive trials). Six of 22 triggered a GDP. Reconstruction of the corresponding EGin is illustrated below (axon, orange; dendrites and soma, black). Scale bar represents 200 μm.

(B2) GDP frequency. Graph plotting the time interval between GDPs (inter-GDP interval) as a function of time in a representative EGin (illustrated below, same as B1) significantly decreasing the GDP occurrence when stimulated (orange).

(B3) Backward phase shift. Same stimulation as (B1) but for a representative EGin inducing a backward GDP phase shift when stimulated. Phase shift is illustrated in graph plotting the number of GDP cycles skipped during phasic stimulation (orange) as a function of time. The number of expected GDPs was calculated during resting conditions (white) based on the average interval between GDPs. Recorded cell is illustrated below (same as B1).

(C) Same as (B), but stimulating LGins. Stimulation of none of the tested LGins perturbed network dynamics significantly despite their fairly developed axonal morphology (green). Tamoxifen induction: E18.5. Analysis: P6–P7.

NOS expression was virtually absent. This constellation of neurochemical expression, axonal labeling of the fimbria, in combination with the regional distribution of their somata (Jinno et al., 2007), strongly suggest that early-born hub neurons most likely develop into GABA projection neurons (Ferraguti et al., 2004; Gulyás et al., 2003; Jinno et al., 2007; Jinno, 2009). Although it would be expected that CA1 septum-projecting interneurons express CB, or CR and NPY, these markers were virtually absent in the EGin population. Perhaps this can be accounted for by species differences (i.e., rat versus mouse).

The finding that GABA projection neurons are the earliest generated is in agreement with the early development of a pioneer GABA pathway from the rat hippocampus, reaching the septum as early as E16 prior to glutamatergic afferents and septohippocampal connections (Linke et al., 1995). It is also compatible with the observation that GDPs, recorded in the septum in the intact septohippocampal complex in vitro, originate in the hippocampus and propagate to the septum via hippocamposeptal-projecting neurons (Leinekugel et al., 1998). Still, the exact extrahippocampal projection pattern of early-born

hub neurons may not be restricted to the septum as GABA projection neurons have been reported to target a variety of structures (Ceranik et al., 1997; Fuentealba et al., 2008; Higo et al., 2009; Jinno et al., 2007; Jinno, 2009; Miyashita and Rockland, 2007). Future retrograde labeling studies of the cells targeted in this study will be required to precisely address this issue. Interestingly, due to their long distance anatomic connectivity and sparseness, GABA neurons with an extrahippocampal projection were already speculated to carry a hub function and provide a wiring economy supporting the emergence of network oscillations in the adult hippocampus at a reasonable cost (Buzsáki et al., 2004).

If the intrahippocampal postsynaptic targets of EGins are not the somata of glutamatergic pyramidal neurons, their exact nature still remains to be elucidated. Interestingly, GABA projection neurons have been previously analyzed in detail at the electron microscopic level at two developmental time points (Gulyás et al., 2003; Jinno, 2009). In CA1 hippocampal slices from juvenile rats, interneurons are their major targets (Gulyás et al., 2003) whereas in adult rats in vivo, these cells were reported to selectively innervate the dendritic shafts of pyramidal cells (Jinno et al., 2007). An initial selective targeting of interneurons by EGins hub neurons would match a previous report suggesting that interneurons are the targets of the first GABA synapses formed in the CA1 hippocampal region (Gozlan and Ben-Ari, 2003). Future studies are needed to test whether GABA neurons are, at least transiently, the main targets of early-born hub neurons, an architecture that would provide ideal conditions for the generation of GDPs.

From the above, it is tempting to conclude that early-generated hub neurons constitute a specific interneuron family. Moreover, it implies a strong genetic predetermination in the development of GABA projection neurons and suggests that in addition to their morphophysiological features (Butt et al., 2005), specialized interneuron function may also be strongly predetermined by embryonic origin. Furthermore, the precocious maturation of hub neurons in principle makes them less susceptible to activity-dependent maturation processes as these cells likely develop in a poorly active environment.

Still, hub cells are not a homogenous interneuron family. Indeed, we had previously described GABA hub neurons with a basket-like axonal pattern (Bonifazi et al., 2009), a population that was not observed in the neurobiotin-filled EGins during our in vitro experiments. Nevertheless, rare EGins were found to be immunopositive for PV in stratum pyramidale or granular layer at P7 and P30, suggesting the presence of occasional PV-positive perisomatic interneurons. The embryonic origin and adult fate of basket-like hub neurons therefore still remains to be determined. This subpopulation of hub neurons may similarly be maintained into adulthood, as perisomatic interneurons with the ability to time the incidence of sharp waves have recently been described in adult hippocampal slices (Ellender et al., 2010). In addition, the population of early-generated hub neurons itself displays some diversity at P7, which persists in adult animals as revealed by the cell reconstructions. Heterogeneity also prevails in the population of GABA projection hippocampal neurons because at least seven different types of them have been previously described (Fuentealba et al., 2008; Jinno et al., 2007). A common embryonic origin may link these various cell types within a family of GABA projecting neurons. Alternatively, different classes of GABA neurons may progressively and transiently function as hub cells at different postnatal stages of development. If true, what we previously grouped as "hub cells" may comprise distinct populations that differentially contribute in the generation of GDPs. Such variety in hub cells could provide functional redundancy that could conceivably protect against developmental insults that impaired particular populations.

EGins Become Hub Cells: Functional Implications

When considering early-born hubs from a functional viewpoint, it is important to stress that they are solely defined by their high connectivity index, which at least theoretically allow them to act as important nodes in the flow of information between populations of neurons. Importantly, they do not create rhythms but merely convey activity to many neurons: hub neurons are not necessarily "pacemakers." In fact, basic electrophysiological characterization of EGins did not reveal any major intrinsic oscillatory mechanism within these cells. These cells are very likely to be synaptically-driven because they display a higher sEPSPs frequency than other GABA neurons. Accordingly, electron microscopy analysis of the synaptic innervation impinging onto GABA projection neurons showed that these cells almost exclusively received glutamatergic synapses (Takács et al., 2008). Understanding whether hub neurons are critical for the production of GDPs in physiological conditions requires approaches enabling their selective and complete elimination. The present results provide a first step toward achieving this technically challenging task.

The finding that EGins are hub cells may imply that, as proposed for other pioneer hippocampal neurons, these cells may provide as molecular cues for the development of layer specific hippocampal and extra-hippocampal afferents (Supèr et al., 1998). Comparison with neocortical development, a region where pioneer neurons have been extensively described, may be particularly instructive. Indeed, besides their early generation, hippocampal hub cells share several remarkable properties with subsets of subplate neurons including: (1) long distance projections (Chun et al., 1987; Kanold and Luhmann, 2010; Luhmann et al., 2009; Tamamaki and Tomioka, 2010; Voigt et al., 2001); (2) mature electrophysiological properties (Hirsch and Luhmann, 2008); (3) the expression of SOM (Chun et al., 1987; Tamamaki and Tomioka, 2010), and GAD67 (Arias et al., 2002); and (4) a role in driving synchronous activity in immature cortical networks (Dupont et al., 2006; Kanold and Luhmann, 2010; Voigt et al., 2001) that identifies the subplate as a "hub station" (Kanold and Luhmann, 2010). Whether hub neurons indeed exist in the developing neocortex and persist into adulthood remains an open question.

The present finding is also interesting from the perspective of pathology. As alluded to above, these cells may provide robustness against pathological insults, in particular those resulting from environmental factors influencing brain development. Interestingly, it was previously shown that the septum-projecting subclass of CA1 SOM-containing neurons is selectively spared in a chronic rat model of Temporal Lobe Epilepsy, indicating that early-born hub neurons may be resistant to epileptogenesis

(Cossart et al., 2001). Whether EGins are central to synchronization processes in epileptic networks therefore remains a viable hypothesis, supported by computational simulations (Morgan and Soltesz, 2008). Now that a subpopulation of hub neurons is accessible to the conditional expression of genes of interest, including optogenetic vectors (Kätzel et al., 2011), the involvement of superconnected neurons in different forms of physiological or pathological oscillations can be explored.

EXPERIMENTAL PROCEDURES

Mice for Inducible Genetic Fate Mapping

All animal use protocols were performed under the guidelines of the French National Ethic Committee for Sciences and Health report on "Ethical Principles for Animal Experimentation" in agreement with the European Community Directive 86/609/EEC.

Double-homozygous *Mash1BAC*$^{CreER/CreER}$/*RCE:LoxP*$^{+/+}$ and *Dlx1/2*$^{CreER/CreER}$/*RCE:LoxP*$^{+/+}$ (Batista-Brito et al., 2008; Miyoshi et al., 2010) male mice were crossed with 7- to 8-week-old wild-type Swiss females (C.E Janvier, France) for offspring production. To induce CreER activity, we administered a tamoxifen solution (Sigma, St. Louis, MO) by gavaging (force-feeding) pregnant mice with a silicon-protected needle (Fine Science Tools, Foster City, CA). We used 2mg of tamoxifen solution per 30 g of body weight prepared at 10 mg/ml in corn oil (Sigma). Pregnant females crossed with *Dlx1/2*$^{CreER/CreER}$/*RCE:LoxP*$^{+/+}$ males were force-fed at embryonic days 7.5 or 9.5 days post vaginal plug (corresponding to the embryonic ages E7.5-E9.5) in order to label early expressing *Dlx1/2* precursors with GFP in the embryos. For simplification purposes GFP expressing mice pups originating from these gavaged females are named tamoxifen-treated *Dlx1/2*^{CreERTM}*;RCE:LoxP*. Similarly, pregnant females crossed with *Mash1BAC*$^{CreER/CreER}$/ *RCE:LoxP*$^{+/+}$ males were gavaged at E18.5, in order to label late expressing *Mash1* precursors in the embryos named *Mash1*^{CreERTM}*;RCE:LoxP* mice.

To assess the temporal precision of EGins labeling, we performed six injections of 5-bromo-2′-deoxyuridine (BrdU, 10 mg/ml in PBS) every 4 hr, starting 6 hr after pregnant mice were force-fed with tamoxifen at E9.5 (50 μg/g intraperitoneally [i.p.]). In another set of experiments, BrdU was injected 31 hr after tamoxifen force-feeding to check that tamoxifen action does not extend over 24 hr. Sections from E12.5 embryos were immunoreacted for both GFP and BrdU as detailed in Figure S1. Similar results were obtained when tamoxifen was force-fed at E7.5 or E9.5 (Figure S1).

Slice Preparation and Calcium Imaging

Horizontal hippocampal slices (380 μm thick) were prepared from 5- to 7-day-old (P5–P7) tamoxifen-treated *Dlx1/2*^{CreERTM}*;RCE:LoxP* (n = 56 slices) or *Mash1*^{CreERTM}*;RCE:LoxP* (n = 39 slices) mouse pups with a Leica VT1200 S vibratome using the Vibrocheck module in ice-cold oxygenated modified artificial cerebrospinal fluid (0.5 mM $CaCl_2$ and 7 mM $MgSO_4$; NaCl replaced by an equimolar concentration of choline). Slices were then transferred for rest (1 hr) in oxygenated normal ACSF containing (in mM): 126 NaCl, 3.5 KCl, 1.2 NaH_2PO_4, 26 $NaHCO_3$, 1.3 $MgCl_2$, 2.0 $CaCl_2$, and 10 D-glucose, pH 7.4. For AM-loading, slices were incubated in a small vial containing 2.5 ml of oxygenated ACSF with 25 μl of a 1 mM Fura2-AM solution (in 100% DMSO) for 20–30 min. Slices were incubated in the dark, and the incubation solution was maintained at 35°–37°C. Slices were perfused with continuously aerated (3 ml/min; O_2/CO_2-95/5%) normal ACSF at 35°C–37°C. Imaging was performed with a multibeam multiphoton pulsed laser scanning system (LaVision Biotech) coupled to a microscope as previously described (Crépel et al., 2007). Images were acquired through a CCD camera, which typically resulted in a time resolution of 50–150 ms per frame. Slices were imaged using a 20×, NA 0.95 objective (Olympus). Imaging depth was on average 80 μm below the surface (range: 50–100 μm).

Electrophysiology

A total of 121 neurons were recorded: 65 were recorded only for morphophysiological characterization in adult slices, whereas 56 were recorded while imaging. Out of the latter, only 32 were considered. The other experiments (n = 24) were discarded because they did not comply either one of the following criteria: (1) stable electrophysiological recordings at resting membrane potential (i.e., the holding current did not change by more than 15 pA); (2) stable network dynamics measured with calcium imaging (i.e., the coefficient of variation of the inter-GDP interval did not exceed 1); (3) complete labeling of the recorded cell; and (4) good quality calcium imaging while recording. Neurons were held in current-clamp using a patch-clamp amplifier (HEKA, EPC10) in the whole-cell configuration. Intracellular solution composition was (in mM): 130 K-methylSO$_4$, 5 KCl, 5 NaCl, 10 HEPES, 2.5 Mg-ATP, 0.3 GTP, and 0.5% neurobiotin. No correction for liquid junction potential was applied. The osmolarity was 265–275 mOsm, pH 7.3. Microelectrodes resistance was 4–8 MOhms. Uncompensated access resistance was monitored throughout the recordings. Values below 20 MOhms were considered acceptable and the results were discarded if it changed by more than 20%. Whole cell measurements were filtered at 3 kHz using a patch-clamp amplifier. Recordings were digitized online (10 kHz) with an interface card to a personal computer and acquired using Axoscope 7.0 software. Spontaneous EPSPs were detected and analyzed using the MiniAnalysis software. For most stimulation experiments, the movie acquisition time was separated evenly between (1) an ~3 min resting period during which the cell was held close to V_{rest} (i.e., zero current injection); (2) an ~3 min stimulation period during which phasic stimulation protocols were applied; and (3) an ~3 min recovery period where the cell was brought back to resting membrane potential. Stimulation protocol: suprathreshold current pulses (amplitude: 100–200 pA, duration: 200 ms) repeated at 0.1–0.2 Hz. V_{rest} was measured as the membrane potential baseline value obtained in current-clamp mode in the absence of current injection. The action potential threshold ($V_{threshold}$) and amplitude, membrane capacitance (C_m), and resistance (R_m) were measured offline using Clampfit. V_{rest} and $V_{threshold}$ were not corrected for errors due to high input resistance values in developing neurons.

Morphology

Neurobiotin Filled Cell Recovering

Slices were fixed overnight at 4°C in Antigenfix, rinsed in PBS containing 0.3% Triton X-100 (PBST) and incubated overnight at room temperature in cy3-streptavidin (1/1000 in PBST). Post hoc analysis was performed using a confocal microscope. Stacks of optical sections were collected for computer-assisted neuron reconstructions.

Immunocytochemistry

Animals were deeply anesthetized with a ketamine (50 mg /ml) and xylazine (7.5 mg /ml) solution at a dose of 2 ml/kg (i.p.) and perfused transcardially with 4% paraformaldehyde in PB (1 ml/g) at a constant flow (2 ml/min). Brains were postfixed overnight in fixative and washed. Horizontal brain sections (40 μm) were routinely processed for multiple immunofluorescence. Briefly, after preincubation in 5% normal donkey serum, sections were incubated in a mixture of primary antibodies from different species, then incubated in appropriate secondary antibodies conjugated with either Al488 (1:500, Molecular Probes; Invitrogen), Cy3, Cy5, DL488, DL549, DL649 (Jackson ImmunoResearch Laboratories) for 2 hr. The dilutions, characteristics, specificity, and sources of primary antibodies are presented in Table S1. Some sections were also processed for GFP immunoperoxidase. No staining corresponding to specific labeling was observed when primary antisera were omitted. In multiple labeling experiments using primary antibodies from different species, the lack of cross-reactivity of the secondary antibodies was consistently checked.

Images were obtained with a Zeiss AxioImager Z2 microscope coupled to a camera (Zeiss AxioCam MR3). Immunofluorescence images were acquired using a halogene HBO lamp associated with (470/40, 525/50), (545/25, 605/70) filter cubes for detection of Al488, Cy3 or DL549, Cy5, or DL649. Counts were performed manually. All results are given as percentages of total number of cells (Figure 1C) or as means of percentages ± SEM (Figures 3L and 3M), n being the number of mice per group.

Morphometric Analysis

Forty-three neurons were reconstructed with a computer assisted system attached to a microscope (Neurolucida, MicroBrightfield). Out of those, 31 were included in the morphometric analysis. Morphological variables

included: dendritic and axonal lengths, dendritic and axonal surfaces, and number of dendritic and axonal terminals. We also performed a Sholl analysis in order to determine the distribution of the number of axonal intersections with circles of increasing radius (20 μm steps) centered at the cell's soma.

Cluster analysis for morphological data was performed using Statistica software. Our analysis was performed with Euclidean distances using Ward's method. According to Ward's method, cases are assigned to clusters so that the variance (sum of squared deviations from the mean) within each cluster is minimized.

Analysis of Network Dynamics

Signal Detection

We used custom designed MATLAB software (Bonifazi et al., 2009) that allowed: (1) automatic identification of loaded cells; (2) measuring the average fluorescence transients from each cell as a function of time; (3) detecting the onsets and offsets of calcium signals; and (4) reconstructing the functional connectivity of the imaged network.

Analysis of Network Synchronizations

Network synchronizations (GDPs) were detected as synchronous onsets peaks including more neurons than expected by chance, as previously described (Bonifazi et al., 2009).

Effective Connectivity Map

In order to identify cells in the network responding to phasic stimulations, for each cell we first calculated the average fluorescence change across trials in a time window between −1 and +1 s centered on the time of the stimulus. Cross-correlation between the average calcium signal of the cell and the calcium signal of the stimulated cell was calculated at time lags varying between −1 and +1 s. If the maximum of the cross-correlation exceeded 0.5 and occurred at positive times, indicating that the activation of the cell followed the stimulation, the cell was considered as responding to the stimulation. In order to color-code the effective connectivity map, we built a matrix from the calcium image of the slice and we assigned to each cell its maximal cross-correlation value. The image was then convolved with a Gaussian of unitary amplitude and 8 μm radius.

Cell-Network Interaction

To establish whether the stimulation of a single neuron was able to influence the occurrence of GDPs we used the same procedure as previously described (Bonifazi et al., 2009).

SUPPLEMENTAL INFORMATION

Supplemental Information includes three figures, one table, and Supplemental Experimental Procedures and can be found with this article online at doi:10.1016/j.neuron.2011.06.018.

ACKNOWLEDGMENTS

We thank Dr. R. Machold for generating the Dlx1/2-creER allele and Dr. J. Johnston for providing the *Mash1*^{CreERTM} mouse. We thank Drs. Y. Ben-Ari and S. Feldt for critical comments. We thank Dr. M. Esclapez for providing occasional access to her Neurolucida system. Research in the Cossart group was supported by grants from the European Research Council (ERC FP7 Young Investigators 242852), the Fondation pour la Recherche Medicale (Equipe FRM 2008), the Fondation Bettencourt Schueller, INSERM, the Ville de Marseille and Region PACA and the FRC. Drs. R. Cossart and A. Baude are funded by the CNRS. Research in the Fishell laboratory is supported by the National Institutes of Health (RO1 grants R01MH071679 and R01NS039007).

Accepted: June 9, 2011
Published: August 24, 2011

REFERENCES

Acsády, L., Görcs, T.J., and Freund, T.F. (1996). Different populations of vasoactive intestinal polypeptide-immunoreactive interneurons are specialized to control pyramidal cells or interneurons in the hippocampus. Neuroscience *73*, 317–334.

Anderson, S.A., Eisenstat, D.D., Shi, L., and Rubenstein, J.L. (1997). Interneuron migration from basal forebrain to neocortex: dependence on Dlx genes. Science *278*, 474–476.

Arias, M.S., Baratta, J., Yu, J., and Robertson, R.T. (2002). Absence of selectivity in the loss of neurons from the developing cortical subplate of the rat. Brain Res. Dev. Brain Res. *139*, 331–335.

Barabasi, A.L., and Albert, R. (1999). Emergence of scaling in random networks. Science *286*, 509–512.

Batista-Brito, R., and Fishell, G. (2009). The developmental integration of cortical interneurons into a functional network. Curr. Top. Dev. Biol. *87*, 81–118.

Batista-Brito, R., Close, J., Machold, R., and Fishell, G. (2008). The distinct temporal origins of olfactory bulb interneuron subtypes. J. Neurosci. *28*, 3966–3975.

Ben-Ari, Y. (2001). Developing networks play a similar melody. Trends Neurosci. *24*, 353–360.

Ben-Ari, Y., Cherubini, E., Corradetti, R., and Gaiarsa, J.L. (1989). Giant synaptic potentials in immature rat CA3 hippocampal neurones. J. Physiol. *416*, 303–325.

Blankenship, A.G., and Feller, M.B. (2010). Mechanisms underlying spontaneous patterned activity in developing neural circuits. Nat. Rev. Neurosci. *11*, 18–29.

Boccaletti, S., Latora, V., Moreno, Y., Chavez, M., and Hwang, D.-U. (2006). Complex networks: structure and dynamics. Phys. Rep. *424*, 175–308.

Bonifazi, P., Goldin, M., Picardo, M.A., Jorquera, I., Cattani, A., Bianconi, G., Represa, A., Ben-Ari, Y., and Cossart, R. (2009). GABAergic hub neurons orchestrate synchrony in developing hippocampal networks. Science *326*, 1419–1424.

Bulfone, A., Wang, F., Hevner, R., Anderson, S., Cutforth, T., Chen, S., Meneses, J., Pedersen, R., Axel, R., and Rubenstein, J.L. (1998). An olfactory sensory map develops in the absence of normal projection neurons or GABAergic interneurons. Neuron *21*, 1273–1282.

Bullmore, E., and Sporns, O. (2009). Complex brain networks: graph theoretical analysis of structural and functional systems. Nat. Rev. Neurosci. *10*, 186–198.

Butt, S.J., Fuccillo, M., Nery, S., Noctor, S., Kriegstein, A., Corbin, J.G., and Fishell, G. (2005). The temporal and spatial origins of cortical interneurons predict their physiological subtype. Neuron *48*, 591–604.

Buzsáki, G., Geisler, C., Henze, D.A., and Wang, X.J. (2004). Interneuron Diversity series: Circuit complexity and axon wiring economy of cortical interneurons. Trends Neurosci. *27*, 186–193.

Ceranik, K., Bender, R., Geiger, J.R.P., Monyer, H., Jonas, P., Frotscher, M., and Lübke, J. (1997). A novel type of GABAergic interneuron connecting the input and the output regions of the hippocampus. J. Neurosci. *17*, 5380–5394.

Chun, J.J., Nakamura, M.J., and Shatz, C.J. (1987). Transient cells of the developing mammalian telencephalon are peptide-immunoreactive neurons. Nature *325*, 617–620.

Cossart, R., Dinocourt, C., Hirsch, J.C., Merchan-Perez, A., De Felipe, J., Ben-Ari, Y., Esclapez, M., and Bernard, C. (2001). Dendritic but not somatic GABAergic inhibition is decreased in experimental epilepsy. Nat. Neurosci. *4*, 52–62.

Crépel, V., Aronov, D., Jorquera, I., Represa, A., Ben-Ari, Y., and Cossart, R. (2007). A parturition-associated nonsynaptic coherent activity pattern in the developing hippocampus. Neuron *54*, 105–120.

Danglot, L., Triller, A., and Marty, S. (2006). The development of hippocampal interneurons in rodents. Hippocampus *16*, 1032–1060.

Del Río, J.A., Heimrich, B., Borrell, V., Förster, E., Drakew, A., Alcántara, S., Nakajima, K., Miyata, T., Ogawa, M., Mikoshiba, K., et al. (1997). A role for Cajal-Retzius cells and *reelin* in the development of hippocampal connections. Nature *385*, 70–74.

Dupont, E., Hanganu, I.L., Kilb, W., Hirsch, S., and Luhmann, H.J. (2006). Rapid developmental switch in the mechanisms driving early cortical columnar networks. Nature *439*, 79–83.

Ellender, T.J., Nissen, W., Colgin, L.L., Mann, E.O., and Paulsen, O. (2010). Priming of hippocampal population bursts by individual perisomatic-targeting interneurons. J. Neurosci. *30*, 5979–5991.

Ferraguti, F., Cobden, P., Pollard, M., Cope, D., Shigemoto, R., Watanabe, M., and Somogyi, P. (2004). Immunolocalization of metabotropic glutamate receptor 1alpha (mGluR1alpha) in distinct classes of interneuron in the CA1 region of the rat hippocampus. Hippocampus *14*, 193–215.

Fuentealba, P., Tomioka, R., Dalezios, Y., Márton, L.F., Studer, M., Rockland, K., Klausberger, T., and Somogyi, P. (2008). Rhythmically active enkephalin-expressing GABAergic cells in the CA1 area of the hippocampus project to the subiculum and preferentially innervate interneurons. J. Neurosci. *28*, 10017–10022.

Garaschuk, O., Hanse, E., and Konnerth, A. (1998). Developmental profile and synaptic origin of early network oscillations in the CA1 region of rat neonatal hippocampus. J. Physiol. *507*, 219–236.

Ghosh, A., and Shatz, C.J. (1992). Involvement of subplate neurons in the formation of ocular dominance columns. Science *255*, 1441–1443.

Gozlan, H., and Ben-Ari, Y. (2003). Interneurons are the source and the targets of the first synapses formed in the rat developing hippocampal circuit. Cereb. Cortex *13*, 684–692.

Gulyás, A.I., Hájos, N., Katona, I., and Freund, T.F. (2003). Interneurons are the local targets of hippocampal inhibitory cells which project to the medial septum. Eur. J. Neurosci. *17*, 1861–1872.

Hennou, S., Khalilov, I., Diabira, D., Ben-Ari, Y., and Gozlan, H. (2002). Early sequential formation of functional GABA(A) and glutamatergic synapses on CA1 interneurons of the rat foetal hippocampus. Eur. J. Neurosci. *16*, 197–208.

Higo, S., Akashi, K., Sakimura, K., and Tamamaki, N. (2009). Subtypes of GABAergic neurons project axons in the neocortex. Front Neuroanat *3*, 25.

Hirsch, S., and Luhmann, H.J. (2008). Pathway-specificity in N-methyl-D-aspartate receptor-mediated synaptic inputs onto subplate neurons. Neuroscience *153*, 1092–1102.

Jinno, S. (2009). Structural organization of long-range GABAergic projection system of the hippocampus. Front Neuroanat *3*, 13.

Jinno, S., Klausberger, T., Marton, L.F., Dalezios, Y., Roberts, J.D., Fuentealba, P., Bushong, E.A., Henze, D., Buzsáki, G., and Somogyi, P. (2007). Neuronal diversity in GABAergic long-range projections from the hippocampus. J. Neurosci. *27*, 8790–8804.

Kanold, P.O., and Luhmann, H.J. (2010). The subplate and early cortical circuits. Annu. Rev. Neurosci. *33*, 23–48.

Kanold, P.O., and Shatz, C.J. (2006). Subplate neurons regulate maturation of cortical inhibition and outcome of ocular dominance plasticity. Neuron *51*, 627–638.

Kätzel, D., Zemelman, B.V., Buetfering, C., Wölfel, M., and Miesenböck, G. (2011). The columnar and laminar organization of inhibitory connections to neocortical excitatory cells. Nat. Neurosci. *14*, 100–107.

Klausberger, T., and Somogyi, P. (2008). Neuronal diversity and temporal dynamics: the unity of hippocampal circuit operations. Science *321*, 53–57.

Leinekugel, X., Khalilov, I., Ben-Ari, Y., and Khazipov, R. (1998). Giant depolarizing potentials: the septal pole of the hippocampus paces the activity of the developing intact septohippocampal complex in vitro. J. Neurosci. *18*, 6349–6357.

Linke, R., Pabst, T., and Frotscher, M. (1995). Development of the hippocamposeptal projection in the rat. J. Comp. Neurol. *351*, 602–616.

Long, J.E., Cobos, I., Potter, G.B., and Rubenstein, J.L. (2009). Dlx1&2 and Mash1 transcription factors control MGE and CGE patterning and differentiation through parallel and overlapping pathways. Cereb. Cortex *19* (*Suppl 1*), i96–i106.

Luhmann, H.J., Kilb, W., and Hanganu-Opatz, I.L. (2009). Subplate cells: amplifiers of neuronal activity in the developing cerebral cortex. Front Neuroanat *3*, 19.

Marín, O., and Rubenstein, J.L. (2001). A long, remarkable journey: tangential migration in the telencephalon. Nat. Rev. Neurosci. *2*, 780–790.

Menendez de la Prida, L., Bolea, S., and Sanchez-Andres, J.V. (1998). Origin of the synchronized network activity in the rabbit developing hippocampus. Eur. J. Neurosci. *10*, 899–906.

Meyer, G., Soria, J.M., Martínez-Galán, J.R., Martín-Clemente, B., and Fairén, A. (1998). Different origins and developmental histories of transient neurons in the marginal zone of the fetal and neonatal rat cortex. J. Comp. Neurol. *397*, 493–518.

Miyashita, T., and Rockland, K.S. (2007). GABAergic projections from the hippocampus to the retrosplenial cortex in the rat. Eur. J. Neurosci. *26*, 1193–1204.

Miyoshi, G., and Fishell, G. (2006). Directing neuron-specific transgene expression in the mouse CNS. Curr. Opin. Neurobiol. *16*, 577–584.

Miyoshi, G., and Fishell, G. (2011). GABAergic interneuron lineages selectively sort into specific cortical layers during early postnatal development. Cereb. Cortex *21*, 845–852.

Miyoshi, G., Butt, S.J., Takebayashi, H., and Fishell, G. (2007). Physiologically distinct temporal cohorts of cortical interneurons arise from telencephalic Olig2-expressing precursors. J. Neurosci. *27*, 7786–7798.

Miyoshi, G., Hjerling-Leffler, J., Karayannis, T., Sousa, V.H., Butt, S.J., Battiste, J., Johnson, J.E., Machold, R.P., and Fishell, G. (2010). Genetic fate mapping reveals that the caudal ganglionic eminence produces a large and diverse population of superficial cortical interneurons. J. Neurosci. *30*, 1582–1594.

Morgan, R.J., and Soltesz, I. (2008). Nonrandom connectivity of the epileptic dentate gyrus predicts a major role for neuronal hubs in seizures. Proc. Natl. Acad. Sci. USA *105*, 6179–6184.

Price, D.J., Aslam, S., Tasker, L., and Gillies, K. (1997). Fates of the earliest generated cells in the developing murine neocortex. J. Comp. Neurol. *377*, 414–422.

Sik, A., Ylinen, A., Penttonen, M., and Buzsáki, G. (1994). Inhibitory CA1-CA3-hilar region feedback in the hippocampus. Science *265*, 1722–1724.

Sik, A., Penttonen, M., Ylinen, A., and Buzsáki, G. (1995). Hippocampal CA1 interneurons: an in vivo intracellular labeling study. J. Neurosci. *15*, 6651–6665.

Sousa, V.H., Miyoshi, G., Hjerling-Leffler, J., Karayannis, T., and Fishell, G. (2009). Characterization of Nkx6-2-derived neocortical interneuron lineages. Cereb. Cortex *19* (*Suppl 1*), i1–i10.

Supèr, H., Martínez, A., Del Río, J.A., and Soriano, E. (1998). Involvement of distinct pioneer neurons in the formation of layer-specific connections in the hippocampus. J. Neurosci. *18*, 4616–4626.

Takács, V.T., Freund, T.F., and Gulyás, A.I. (2008). Types and synaptic connections of hippocampal inhibitory neurons reciprocally connected with the medial septum. Eur. J. Neurosci. *28*, 148–164.

Tamamaki, N., and Tomioka, R. (2010). Long-range GABAergic connections distributed throughout the neocortex and their possible function. Front Neurosci *4*, 202.

Tricoire, L., Pelkey, K.A., Daw, M.I., Sousa, V.H., Miyoshi, G., Jeffries, B., Cauli, B., Fishell, G., and McBain, C.J. (2010). Common origins of hippocampal Ivy and nitric oxide synthase expressing neurogliaform cells. J. Neurosci. *30*, 2165–2176.

Voigt, T., Opitz, T., and de Lima, A.D. (2001). Synchronous oscillatory activity in immature cortical network is driven by GABAergic preplate neurons. J. Neurosci. *21*, 8895–8905.

Neuron, Volume *71*

Supplemental Information

Pioneer GABA Cells Comprise a Subpopulation of Hub Neurons in the Developing Hippocampus

Michel Aimé Picardo, Philippe Guigue, Paolo Bonifazi, Renata Batista-Brito, Camille Allene, Alain Ribas, Gord Fishell, Agnès Baude, and Rosa Cossart

Supplemental Inventory

Supplemental Figures

Figure S1 related to Figures 1,2 and 4
Figure S2 related to Figure 3
Figure S3 related to Figures 3 and 4
Table S1 related to Figures 1, 2 and 3

Supplemental Experimental Procedures

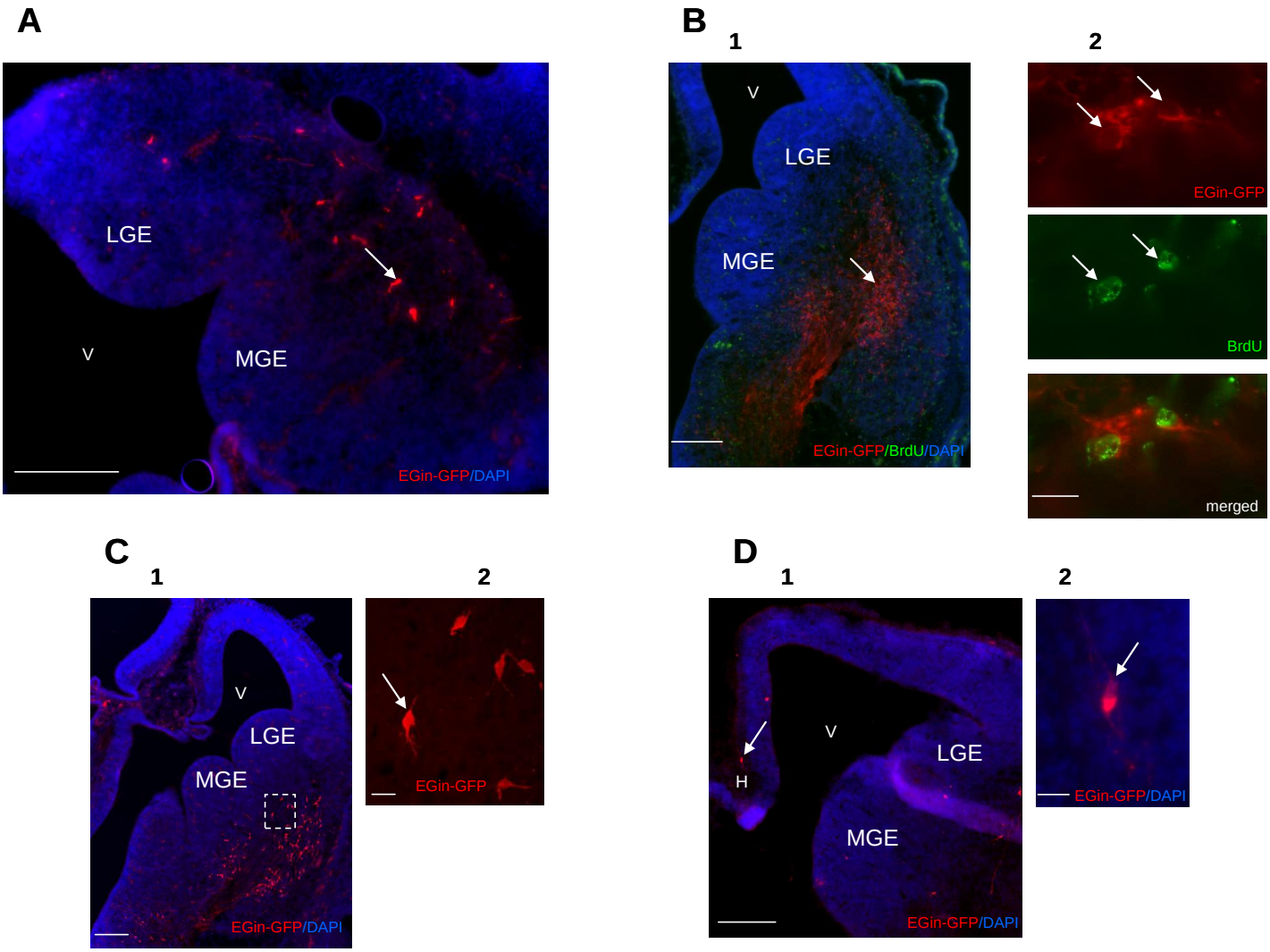

Figure S1. Short-Term Fate Mapping of Dlx1/2 Progenitors

(A) Immunohistochemical analysis of E12.5 embryos extracted from *Dlx1/2*^{CreERTM}*;RCE:LoxP* pregnant mice (tamoxifen-treated at E7.5). EGins (red, e.g. arrow) are found out of the proliferative regions of the lateral and medial ganglionic eminences (LGE and MGE, respectively). V: Ventricule.

(B1) Immunohistochemical analysis of E12.5 embryos extracted from *Dlx1/2*^{CreERTM}*;RCE:LoxP* pregnant mice (tamoxifen-treated at E9.5 and injected with BrdU 6 hours after tamoxifen, see methods) shows EGins are found out of the proliferative regions of LGE and MGE(e.g. arrow).

(B2) High magnification display of two EGins (red, arrows) that are also BrdU positive (green).

(C1) Same as (B) without BrdU treatment.

(C2) High magnification display of C1 highlighted area. In the absence of BrdU treatment, GFP labelling of EGins is of better quality and enables the visualization of fine processes.

(D1) Putatively migrating EGins (tamoxifen injection at E7.5) can be already found at E12.5 near the hippocampal neuroepithelium (H).

(D2) High magnification of D1. Scale bars are: 200 µm (A, B1, C1 & D1), 10 µm (B2), 20 µm (C2 & D2).

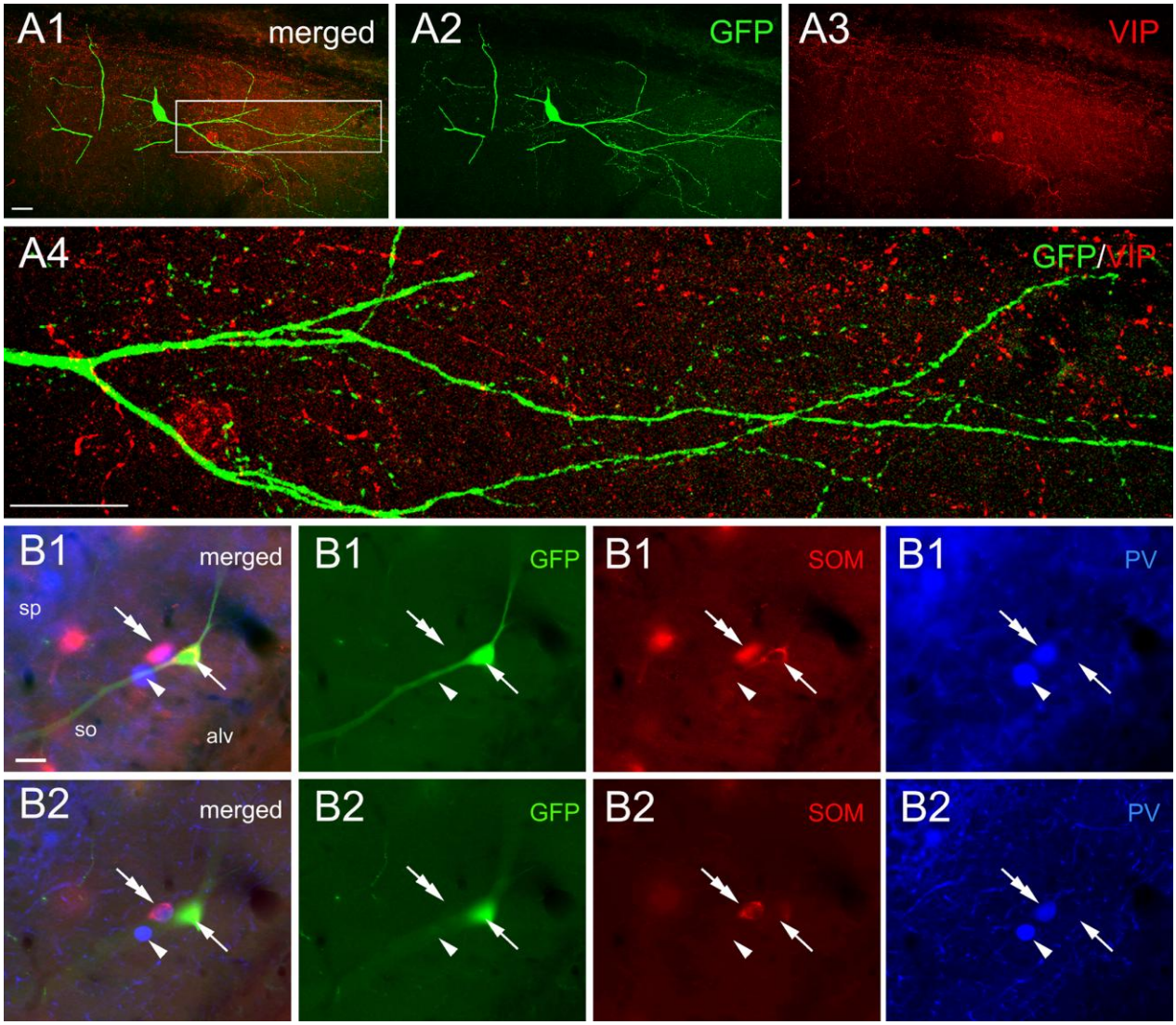

Figure S2. Immunohistochemical Analysis Excludes that a Large Number of Early Generated Neurons Become O-LM Cells

(A) Somata and dendrites of EGins do not receive strong inputs from VIP positive axon terminals (arrows in A; A4 is an enlargement of the boxed area in A1) as shown by the illustrated maximal intensity z projection of confocal microscope views of an EGin within the CA1 stratum oriens.

(B) A somatostatin (SOM) positive EGin (arrow in B) is not positive for parvalbumin (PV, double arrows and arrow head in B) albeit a SOM and PV positive neuron (double arrows) is observed aside. Scale bars are 20 µm. alv, alveus; sp, stratum pyramidale; so, stratum oriens.

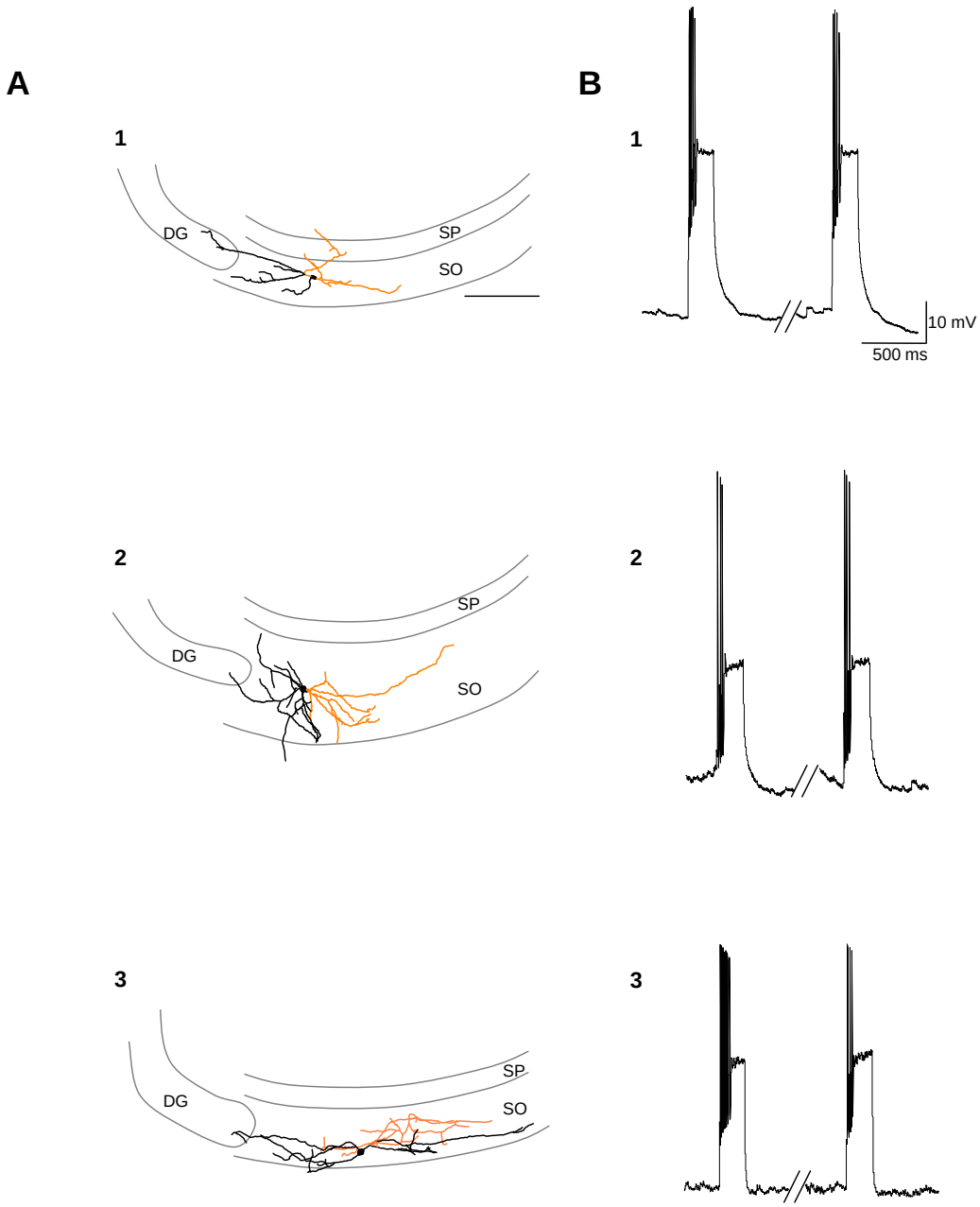

Figure S3. Morphophysiological Properties of EGins Recorded in the CA3 Stratum Oriens of Adult Tamoxifen-Treated (E7.5) *Dlx1/2*^{CreERTM}*;RCE:LoxP* Mice (P30)

(A) Neurolucida reconstructions of three typical EGins filled with neurobiotin. Axonal arborisation: orange; dendrites and cell body: black Scale bar is 200 µm.

(B) Action potential discharge patterns of the cells illustrated on the right, evoked in current-clamp mode, at resting membrane potential, by a current injection step (150 pA, 200 ms).

Table S1. List of Primary Antibodies

Antibody	Host	Source	Characterisation	Immunogens
GFP	Rabbit	Invitrogen, A6455	Specificity analysis assessed by manufacturer.[1]	Native GFP
GFP	Chicken	Aves Labs, GFP-1020	Specificity analysis assessed by manufacturer.	Recombinant GFP
SOM	Rat	Millipore, MAB 354	Labelling pattern as published with other antibodies. Absorption tested by manufacturer with other peptides.[2]	Synthetic peptide 1-14 aa
mGluR1α	Guinea Pig	Frontier Institut, mGluR1a-GP-Af660-1	In WB the AB recognizes a single protein band at 145kDa with not cross reactivity to mGluR5.[3]	Mouse mGluR1 945-1127aa
PV	Mouse	Sigma, P3088	In WB the AB recognizes a band at 12kDa1. Labelling pattern as published with other antibodies.[6]	Purified frog muscle PV
PV	Goat	Swant, PVG-214	Labelling pattern as published with other antibodies.[7]	Purified rat muscle PV
CB	Guinea Pig	Synaptic Systems, 214 004	In WB the AB recognizes a band at 28kDa. Labeling pattern as published with other antibodies[8]	Recombinant protein of human CB 3-251 aa
CR	Goat	Swant, CG1	Labelling pattern as published with other antibodies[9]	Human recombinant CR
M2R	Rat	Synaptic Systems, 223 017	In WB the AB recognizes a band at ~59kDa. No labelling in M2R KO mice[4, 5]	Recombinant protein of human M2R 207-388 aa
NOS	Mouse	Sigma, N 2280	In WB the AB recognizes a band at ~150-160kDa2. Labeling pattern as published with other antibodies[10]	Rat brain recombinant nNOS
NPY	Rabbit	ImmunoStar, 22940	Labelling pattern as published with other antibodies. Absorption tested by manufacturer with 6 other peptides.[11]	Native NPY
VIP	Guinea Pig	Peninsula Lab Bachem, T-5030	Labeling pattern as published with other antibodies. Absorption tested by manufacturer with 8 other peptides.[12]	Synthetic peptide
BrdU	Rat	AbD, OBT0030	Specificity analysis assessed by manufacturer.[13]	Clone BU1/75 (ICR1).

1 Invitrogen, Ltd; http://products.invitrogen.com/ivgn/product/A6455?ICID=search-a6455;
2 Millipore Corp; http://www.millipore.com/catalogue/item/mab354;
3 FRONTIER SCIENCE Co.,Ltd ; http://www.frontier-science.co.jp/PDF/mGluR1a-GP-Af660.pdf;
4 Duttaroy et al., 2002, Mol Pharmacol, 65, 1084-1093;
5 Synaptic Sytems; http://www.sysy.com/products/m-achr-2/facts-223017.php; http://www.sysy.com/products/m-achr-2/223017-blot.html;
6 Sigma Aldrich, Inc;
http://www.sigmaaldrich.com/etc/medialib/docs/Sigma/Datasheet/5/p3088dat.Par.0001.File.tmp/p3088dat.pdf;
7 Swant; http://www.swant.com/pfd/Goat_anti_Parvalbumin2010.pdf;
8 Synaptic Sytems; http://www.sysy.com/products/calbindin/facts-214004.php?n=Calbindins;
http://www.sysy.com/products/calbindin/214004-blot.html;
9 Swant®; http://www.swant.com/pfd/Goat%20anti%20Calretinin%20CG1.pdf;
10 Sigma Aldrich, Inc;
http://www.sigmaaldrich.com/etc/medialib/docs/Sigma/Datasheet/4/n2280dat.Par.0001.File.tmp/n2280dat.pdf;
11 http://www.immunostar.com/content/pdf/22940-812001.pdf;
12 http://www.bachem.com; 13 http://www.abdserotec.com/catalog/datasheet-OBT0030S.html.

Supplemental Experimental Procedures

BrdU Labelling

To assess the temporal precision of EGins labelling, we performed six injections of 5-Bromo-2'-deoxyuridine (BrdU, 10mg/ml in PBS) every 4 hrs, starting 6 hrs after pregnant mice were force-fed with tamoxifen at E9.5 (50 µg/g i.p.). E12.5 embryos were extracted, postfixed 2 hrs “in toto” in Antigenfix (Diapath), cryoprotected (sucrose 30% in saline phosphate buffer -0.1 M PBS, pH 7.4- 12hrs), frozen in liquid nitrogen vapors. Horizontal sections (20 µm) of embryos’ heads were cut with a cryostat (Leica CM 3050S) and GFP was immunoreacted for DL545 fluorescence as described below. Slices were then dipped into Antigenfix (30 min), rinsed in PBS, and treated (30 min, 37°C) with HCl 2N in PBS containing 0.5% triton X-100. After rinsing in sodium tetraborate buffer (0.1M, pH 8.5), slices were processed for DL488 immunofluorescence against BrdU (Sup. Table 1). In another set of experiments BrdU was injected 31 hrs after tamoxifen force-feeding to check that tamoxifen action does not extend over 24 hrs. Similar results were obtained when tamoxifen was force-fed at E7.5 or E9.5 (Fig. S1).

Immunocytochemistry

All mice were perfused through the heart with 4% paraformaldehyde in PB (1ml/g of mice) at a constant flow (2 ml／min). Brains were extracted immediately after perfusion and post-fixed overnight in fixative. After extensive washes horizontal brain sections (40µm) were obtained with a vibratome and stored in PB supplemented with sodium azide (0.05%) until immunostaining procedures. Immunofluorescence was performed on free-floating sections as follows. After incubation for 45 min in 5% normal donkey serum (Jackson ImmunoResearch Laboratories Inc., West Grove, PA, USA) in PBST, sections were sequentially incubated with various primary antibodies diluted in PBS overnight at 4°C; the dilutions, characteristics, specificity and sources of the primary antibodies are presented in supplementary Table 1. Next, sections were incubated in appropriate secondary antibodies conjugated with either Alexa Fluor 488 (1:500, Molecular Probes; Invitrogen), Cy3, Cy5, DyLight 488, DyLight 549, DyLight 649 (Jackson ImmunoResearch Laboratories Inc.) for 2 h. Finally, sections were mounted on slides and cover-slipped using glycerol／PB (0.2 m; 50:50) as mounting medium. Some sections were also processed for immunoperoxydase against GFP. Briefly, after incubation in normal donkey serum, sections were sequentially incubated with primary antibody to GFP in PBS overnight, in biotinylated secondary antibodies (donkey anti-rabbit IgG, 1:50; Jackson ImmunoResearch Laboratories Inc.) and finally in avidin-biotin peroxidase complex (ABC kit; Vector Laboratories Inc., Burlingame, CA, USA). Peroxidase labeling was revealed using 3,3’-diaminobenzidine tetrahydrochloride (0.05% in PB) and hydrogen peroxide (0.01%).